BloomBeacon: Blooming Physical Touch Display Surfaces via Persistence-of-Vision Motion

Willa Yunqi Yang
University of Chicago
Chicago, Illinois, USA
yunqiy@uchicago.edu

Justice T Andersen*
University of Chicago
Chicago, Illinois, USA
jtandersen@uchicago.edu

David Dajun Yuan*
University of Chicago
Chicago, Illinois, USA
dajuny@uchicago.edu

Ken Nakagaki
University of Chicago
Chicago, Illinois, USA
knakagaki@uchicago.edu

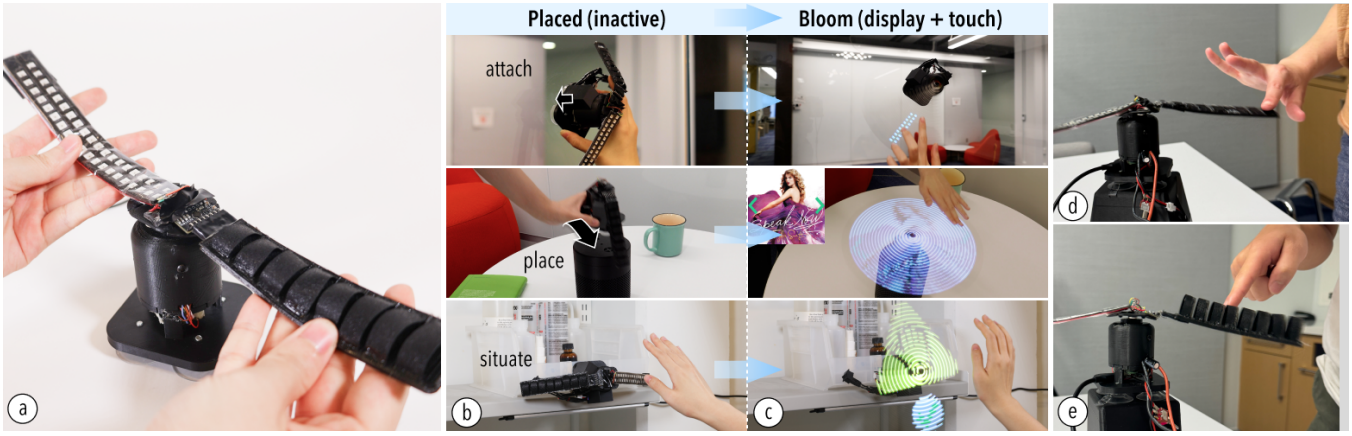


Figure 1: (a) BloomBeacon is a mobile, expansive touch display based on Persistence-of-Vision motion that 'blooms' from soft, line-like blades. When inactive, it is relatively compact, allowing it to be (b) easily placed in the environment. (c) When blooming, a touch surface emerges from the line. (d-e) A series of studies was conducted to investigate the key factors that affect touch-sensing performance and user experience.

Abstract

We explore how a display surface can physically emerge on demand to support both mid-air visualization and direct touch interaction. We introduce blooming, a concept that repurposes Persistence-of-Vision (POV) motion to deploy a large, touchable surface from a compact, relocatable device. Using a soft, rotating line with arch-shaped electrodes, our system renders dynamic mid-air visuals while enabling direct touch input on the manifested surface. Realizing this concept requires addressing the unique challenges of touching spinning elements, including ensuring safety, minimizing disturbances to rotation caused by touch, and detecting brief unstable touches during spinning. We present a safety-oriented device design, special blades effective in minimizing finger disturbance, and optimization techniques tailored to transient, noisy touches. We also reveal how rotation speed and electrode height significantly affect sensing accuracy and user experience. Finally, we demonstrate applications that show how blooming touch displays can flexibly augment everyday objects and environments.

*Contributed equally to this work.

This work is licensed under a Creative Commons Attribution 4.0 International License.

CHI '26, Barcelona, Spain

© 2026 Copyright held by the owner/author(s).

ACM ISBN 979-8-4007-2278-3/26/04
https://doi.org/10.1145/3772318.3790357

CCS Concepts

• **Human-centered computing** → **Touch screens**.

Keywords

Mid-Air Display, Direct Touch, Persistence-of-Vision Display, Environmental Augmentation

ACM Reference Format:
Willa Yunqi Yang, Justice T Andersen, David Dajun Yuan, and Ken Nakagaki. 2026. BloomBeacon: Blooming Physical Touch Display Surfaces via Persistence-of-Vision Motion. In *Proceedings of the 2026 CHI Conference on Human Factors in Computing Systems (CHI '26), April 13–17, 2026, Barcelona, Spain.* ACM, New York, NY, USA, 19 pages. https://doi.org/10.1145/3772318.3790357

1 Introduction

How can we make display surfaces *physically emerge* on demand—not only to display information but also to support *direct touch* interaction? Science fiction movies have long envisioned such scenarios. For example, as illustrated in *Iron Man*'s workshop[1] or Black Panther's wrist UI[2], mid-air display surfaces appear from a single point to dynamically display information while providing touch interaction, and collapse when not in use.

Mid-air display technologies (e.g., employing fog/mist [5, 21, 30, 34], water droplets [10], and styrofoam particles [46]) have

[1]Iron Man 2
[2]Black Panther: Wakanda Forever

been explored to serve such (dis)appearable display surfaces, which allow digital content to seamlessly blend into our physical environments. However, their touch interaction capabilities are often limited — fingers *pass through empty air* (or at best make contact with 'imperceptible' particles), lacking direct physical contact with the displayed information. Such direct physical contact has been widely recognized as important by haptics and HCI communities. While recent advances in mid-air displays have introduced tactile feedback into their systems, they usually require dedicated haptic equipment (e.g. a device that generates ultrasonic beams [35]), or additional computational processes (e.g., acoustic multiplexing [26]) to simulate such feedback. Without having to specifically *simulate contact feedback*, we ask how mid-air display itself could form a physical surface that is directly touchable, while remaining fully integrated into a single compact device.

In this paper, we present the concept of a *blooming* touch display: a compact, relocatable device that leverages the tangible and expansive effects of fast rotation and mid-air visuals through the Persistence of Vision (POV) effect [14]. Using a soft, spinning line, it not only renders rich visuals but also manifests a touch-sensing surface on demand. Such a 'blooming' touch display holds strong potential **for users to augment their environments**: as illustrated in Figure 2, when inactive, the device is mobile and relocatable, allowing users to flexibly place it on everyday surfaces and objects. When active, rotation enables a large expansion ratio from before to after. Our concept broadens the possibility of *where* interactive content can be placed, pop up, and be tangibly interacted with.

To achieve the proposed concept, we identify and articulate the unique and inherent challenges of touching spinning elements, which involve complex, mutually affecting dynamics: rotation making touch unsafe, touch disturbing rotation, and and the difficulties of sensing transient, unstable touches. To tackle these challenges, BloomBeacon integrates safety-oriented device design, arch-shaped electrodes as 'touch buffers' to reduce disturbance from finger contact, and optimization techniques tailored to touches on spinning elements. These serve as generalizable system design heuristics for POV-based touch displays. Beyond the system itself, we also studied the impact of key factors — rotation speed and electrode height — on sensing performance (Figure 1d, e), informing fellow researchers and engineers of generalizable insights beyond a single device implementation. As the initial step that articulates the challenges and develops designs that directly tackle them, our findings pave the way for building future POV-based touch displays toward 'blooming' interactive surfaces in our physical space.

In summary, our contributions are as follows:

- A concept of manifesting a touch display by 'blooming,' supported by a proof-of-concept implementation of POV-based touch display that is safety-oriented, disturbance-minimizing, and touch-sensing-enabled.
- Technical evaluation and user study that characterize the system performance and reveal the impact of rotation speed and electrode height on touch sensing accuracy and user experience.
- A set of applications including soft-surface interactions, physical objects augmentation, pop-up mid-air displays, and overlaying graphical content onto physical environments.

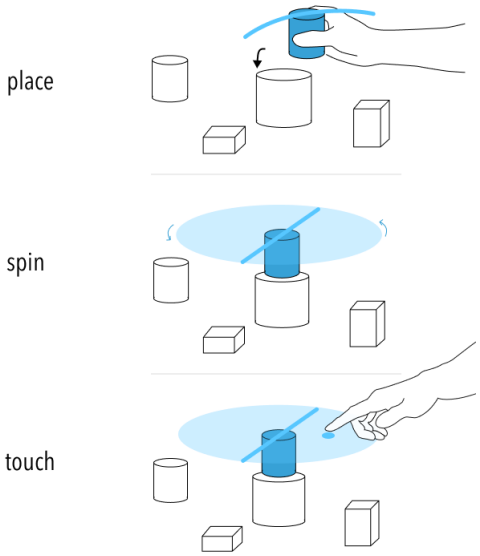


Figure 2: Concept illustration of using a blooming touch display to augment everyday objects.

2 Related Work

2.1 On-Demand Formation of Touch Displays

HCI researchers have been extending the places where digital information can be shown beyond traditional screens. Among the approaches that do not require users to wear any device, projection is one of the major methods, featuring the deployment of a much larger display area compared to the device size. This approach appropriates existing surfaces for touch displays [24, 39, 51]. However, projecting onto the environment introduces a high environmental dependency, including lighting, surface size, color, transparency, and occlusion of the line-of-sight, making this approach vulnerable in diverse everyday environments.

Going beyond existing surfaces from our environment, researchers have been exploring how to *form* a display medium in mid-air. One approach is to create *particles floating in the air*, such as fog [5, 30, 42], water droplets [10], and airborne particles [46] and project images onto them. This approach, however, struggles to provide physical contact when fingers just pass through the 'imperceptible' particles. Recently, breakthroughs in acoustic levitation for volumetric displays have enabled complex visuals combined with projections from the rapid movement of single [26] and multiple particles [40]. Within the same acoustic display, tactile feedback can also be separately generated at close proximity to the display particle via acoustic multiplexing to simulate contact sensation [26]. Other mid-air visualization approaches use additional haptic equipment for contact sensation. For example, in optical and reflective systems that engineer light to form images in mid-air [1, 25, 32, 56], haptic equipment that emits ultrasonic beams for hands can be added to simulate the sensation of physical contact [35].

Most existing approaches to forming touch displays rely on generating tactile feedback separately, either by computationally controlling and simulating the tactile layer within the system or by

using additional haptic equipment. In this work, we explore how to directly manifest a surface that naturally enables physical contact, and we focus on making such a formation more flexible to broaden the reach of touch interfaces in our everyday environments.

2.2 Deployable Structures for UIs and Displays

Employing deployable, expandable mechanisms to create physical UIs and displays has been actively explored in the realm of shape-changing interfaces [7, 43]. The term 'deployable' is often used to describe such interfaces, where [41] defines: "Deployable shape-changing mechanisms enable structures and devices to be stowed for transport or easy handling and expanded when required." Scissor mechanisms are one example that deploy and expand to offer tangible interaction, while being able to be collapsed to compact form factors [52]. Mechanisms that allow devices to be transported more easily, such as rolling and folding, are gaining popularity and transforming our digital experiences as well, such as gaming experiences that are enhanced by portable mobile devices such as rollable gaming mats [50] or foldable phones [2] that expand the mobility and interaction opportunities of flat screens [45]. In Emergeables [44], Robinson et al. proposed the concept of physical, tangible UIs emerging from display surfaces for eyes-free interaction via arrays of actuated mechanisms. Some devices adopt modular, compact designs that allow users to augment physical objects with minimal effort, such as imparting motion by attaching a torque module [55] or enhancing textiles by ironing on interactive patches [58].

Contrasting to the above research, we offer a compactly stored, integrated electrical and mechanical display and sensing system that can 'bloom' to render an interactive touch display. Compared to most deployable, tangible systems, our approach leverages motion to achieve minimal bulk while supporting both visuals and touch sensing within a single system.

2.3 Persistence of Vision Displays

2.3.1 Interaction with Persistence of Vision Displays. Fast speeds and illusory effects have been used as a "deployable mechanism" to create stunning visuals, such as using high-speed projection supported by actuated materials [57] to create realistic displays and rotating fans [29] to allow user-manipulable 3D displays.

Building on fast motion, Persistence of Vision (POV) is the visual illusion where the eye briefly retains an image after it disappears, allowing rapidly flashed static frames to appear continuous. While this phenomenon underlies all animation and videos, POV displays [38] specifically use fast-moving, controlled points of light (e.g., LEDs) to form complete, continuous visuals through motion. For example, spinning one row of LEDs on a fan forms a fan display [6, 38]. Other fast motions, such as vibration [27] and even hand-waving [3, 8], can also provide enough speed for the emitted lights to persist and form images. POV displays have also been appropriated to enable levitated spherical displays (iSphere [53]), to extend smartphones' interactivity [49], and to facilitate face-to-face touch interaction via a double-sided transparent display [31].

Different from a conventional screen, where the black screen sets apart physical surroundings and digital contents, a POV display render "floating" visuals where the background appears transparent. This unique effect of the POV display blurs the boundary between digital contents and their physical surroundings, making the visuals appear in mid-air on our desk, shelf, hallway, and other parts of our physical environment. However, despite their unique visual effects and deployability, existing POV displays are rarely positioned close to users due to their fast-moving rigid elements, let alone being designed for direct touch. To enable touch interaction, Janus [31] sandwiched the rotating elements between touch-sensing-enabled transparent panels where touch occurs. However, this approach requires installing panels and separate sensing equipment, making it stationary and bulky in the environment.

An inspiring work closely related to ours is [49], which focuses on extending smartphones' display capabilities. It shows that a manually spun phone can produce simple POV interactions, but it remains limited: the rotation is inconsistent and momentary, and the smartphone form factor (rigid, short, heavy, and non-configurable) restricts further engineering advances. It provides feasibility but not a pathway for systematically improving POV-based touch displays. In our work, we engineer a motorized, expansive system from the ground up, allowing us to study and intervene in the fundamental challenges of POV-based touch displays. Our end-to-end designed device allows hardware flexibility, safety-oriented mechanics, soft electrodes, and sensing configurations. These are hard to retrofit onto a smartphone platform. This expanded design and engineering space is what allows us to derive generalizable insights and advance the concept of a blooming touch display beyond feasibility.

2.3.2 Non-Rigid Components for Direct Interaction with Fast-Moving Devices. Touching parts in motion has raised known safety concerns [7, 19, 48]. Recent breakthroughs in HCI have proven the feasibility and usability of such kinetic interfaces by making their moving components soft, safe to touch, and allowing touch sensing. For example, traditional volumetric displays can only take input via indirect methods like a mouse or gestures outside of the display. Recently, FlexiVol [13] has replaced the rigid moving diffusers of a volumetric display with soft elastic strips to allow reach-through interaction inside the display. POV displays are also based on fast motion, and their interactivity has been constrained by rigid blades and a lack of integrated touch input. Our work advances this space by introducing a soft, touch-sensing POV device design, addressing both safety and direct interactivity. While FlexiVol inspired us to employ soft materials to allow touch interaction with fast-moving components, our approach to apply this to spinning-POV displays opens up a new category of device — a mobile, relocatable, 'blooming' touch display, allowing users to flexibly place the device to manifest touch display surfaces to augment our physical space.

3 Designing BloomBeacon

3.1 Touching and Sensing on a Motorized Spinning Interface: Challenges and Design Considerations

The concept of *blooming* interactive surfaces is enabled by a motorized spinning display that leverages the tangible and expansive effects of fast rotation. This rotation allows our device to be mobile and relatively compact when inactive, for flexible placement in the environment, and to be expansive on demand.

However, touching a rotating object is uncommon and usually considered unsafe, let alone enabling touch sensing. Touch itself can also disturb the rotation. These considerations reveal complex, mutually affecting dynamics that pose challenges in POV-based touch displays. Below, we structure and articulate these challenges in three layers (Figure 3): rotation affects touch, touch affects rotation, and transient, unstable touch during spinning.

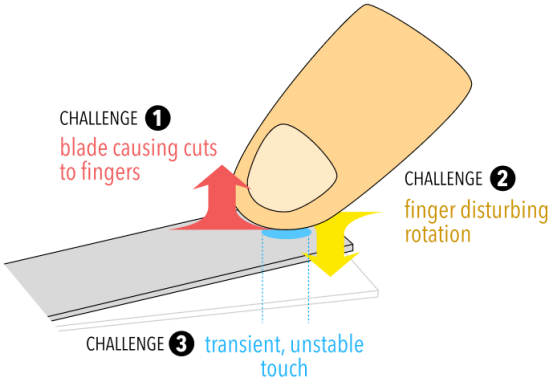


Figure 3: Challenge 1: rotation affects touch (blade causing cuts to the finger). Challenge 2: touch affects rotation (finger disturbing rotation). Challenge 3: transient, unstable touch.

Challenge 1 <C1>. Rotation affects touch: blade causing cuts to the finger. The primary concern when it comes to touching spinning elements is accidental finger reach-throughs. If not designed properly, the fast-spinning blade may cause cuts. The design goal, therefore, is twofold: to ensure that the blades are safe to touch even during fast motion, and to maintain a "weak" rotation with low torque that can be safely interfered with by a finger.
Challenge 2 <C2>. Touch affects rotation: finger disturbing rotation. At the same time, robust POV displays rely on consistent rotation speeds. Direct finger contact, however, can easily disturb the rotation. Therefore, another design goal is to minimize the disturbance from finger contact to maintain a consistent rotation. These two requirements naturally create a tension: safety requires a rotation that is *easily disturbable*, while display robustness requires the rotation to be *minimally disturbed*. Advancing POV touch displays requires a solution that navigates this inherent tension.
Challenge 3 <C3>. During contact: transient, unstable touch. Unlike on conventional screens, where touch is stable and continuous, touching a fast-spinning blade instead creates a series of brief, unstable, intermittent encounters as the blade repeatedly passes the finger. Each pass only allows a brief sensing window (e.g., at 450 RPM, a 10° touch region only spans 3.7ms), and contact quality is affected by partial contact, vibration, material deformation, etc. At the same time, these transient contacts occur among significant noise from rotation, airflow, and disturbances created by the touch itself. There need to be sensing techniques for these characteristics that traditional capacitive sensors aren't optimized to handle.

Although prior work [49] has demonstrated the feasibility of touching a manually spun smartphone with preliminary touch sensing results, these challenges, caused by the complex dynamics, remain underexplored, especially under our concept of blooming a touch display, which requires active actuation. As an initial exploration, our goal is not to prescribe a single optimal hardware configuration. Rather, we use our implementation to illustrate the broader design heuristics, key parameters, and optimization directions for such systems.

Throughout the paper, we address safety around **<C1>** with motor parameters, hinged design, and soft blade in Section 3; a physics model for safety assessment in Section 5.1; and additional safety features in Section 9.1. We highlight our novel design to tackle **<C2>** with soft, arched electrodes in Section 3.4, proven effective across most measured metrics in Section 7. We also detail the sensing techniques tailored to **<C3>** in Section 4 and reveal two key factors influencing sensing performance in Section 5 and 7.

3.2 Hardware Architecture

In this section, we endeavor to provide an overview of our proof-of-concept implementation while detailing how our specific design tackles each of the aforementioned challenges.

Figure 4a illustrates the overall hardware architecture: the base includes a mount with suction cups and a microcontroller (XIAO ESP32S3). Above the base is a BLDC motor and a slip ring that maintains wired connections between the microcontroller and the electronics on the top plate. The top plate is the *spinning assembly* that consists of an LED blade and a sensing blade. The size of the core hardware is $4.5cm \times 4.5cm \times 6cm$, with a $6.5cm \times 6.5cm \times 1cm$ suction cup base. It weighs 120g without battery (207g with battery), and creates a display with a diameter of $30cm$. The current device size is constrained by the motor, suction cups, and the slip ring height. Alternative implementations, such as employing wireless power transmission coils, could potentially reduce the device size.

It is critical for the motor of our display to be low-torque for safety **<C1>**. A low-torque motor's rotation tends to be safely and easily stalled by accidental finger reach-throughs, while a high-torque motor tends to hit the finger when it persists on rotating. Brushless DC motors are preferred over brushed or geared ones for better safety and power efficiency. The motor we use is Vertiq-23-06-G (220kV). The speed that we cap the motor at is 550 RPM (coming from 2.5V to drive the motor). The torque generated by the motor itself at this speed is less than 0.03 Nm.

Another safety-oriented feature is the hinged design of the blades (Figure 6d) **<C1>**. It has several benefits: the blades would be pressed down more easily when there is contact from above, making finger reach-throughs harder. It is also a passive deployable mechanism. When the device is inactive, the blades naturally fall down. Upon rotation, centrifugal force lifts them up to their operational height.

In the following sections, we will detail the spinning assembly: an LED blade and a sensing blade, illustrated in Figure 6a and b.

3.3 LED Blade for Display

We adopted a conventional workflow for building the display part of the POV system [4]. To render a static image using LED strips, the image first needs to be segmented along two axes: the angular axis and the radial axis (Figure 5a).

Along the angular axis, the image is divided into N slices. For example, $N = 180$ slices spun at 550 RPM yield 2 degrees per slice and 606 microseconds per slice. Each slice's angular position is

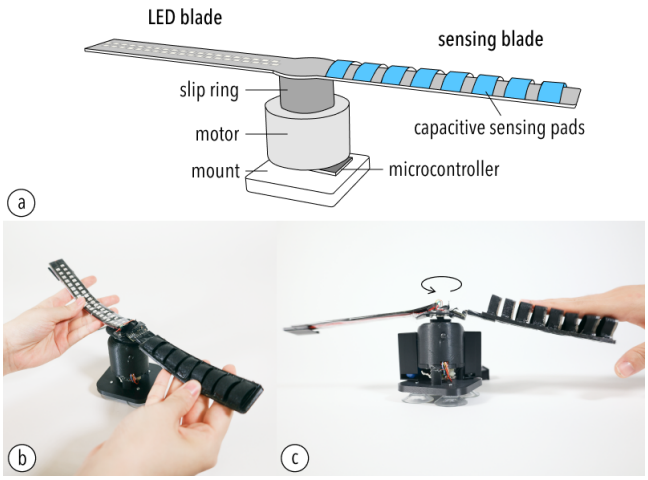


Figure 4: BloomBeacon: (a) System Diagram; (b) Bendable Blades; (c) Soft Electrode Archs

computed by dividing the duration of one revolution by N. The 0° reference point is determined by a digital hall sensor (A3144) mounted on the static base and a magnet attached below the spinning plate. As this 0° reference point is critical to both display and touch accuracy, the digital hall sensor is attached to an interrupt in the program to guarantee its high priority.

Along the radial axis, the resolution is determined by the number of LEDs. A 40-LED strip segments the radius into 40 units.

At runtime, LEDs emit the correct colors at each slice interval. As slices of the image are rapidly formed during the rotation, they persist in our brain to form a continuous image. While the resolution of the display is theoretically determined by the number of slices on the angular axis and the number of LEDs on the radial axis, it is practically constrained by the microcontroller and control speed.

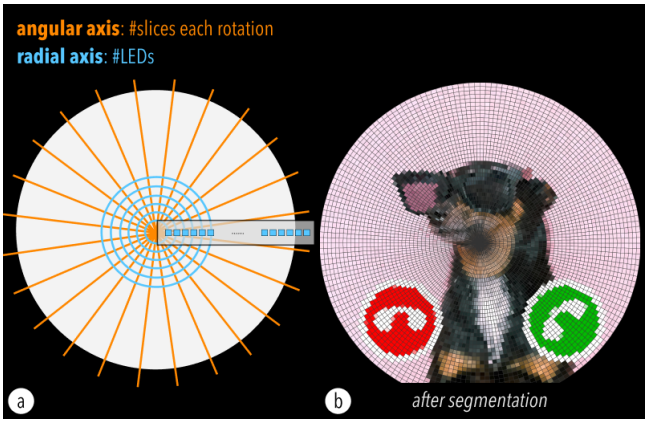


Figure 5: (a) An image is segmented along its angular and radial axis; (b) The interface image after segmentation

POV displays require high-refresh-rate LEDs, so we use high-speed addressable DotStar LEDs, supported by the FastLED Library. For the proof-of-concept, we use the off-the-shelf DotStar LED strip (APA102-5050) where each LED is 5*mm* wide on a formable PCB (can be bent). We offset two 20-LED strips to double the resolution. In general, resolution shouldn't be a concern as DotStar already has 2*mm* wide LEDs (APA102–2020) that can be made into a strip, and advancement in LED miniaturization is forthcoming.

Finally, the edges of the LEDs are rigid and unsafe for direct touch under high rotation speed. Therefore, we designed a 3D printed soft casing with Ninjaflex TPU [54] that encloses the LED strip, making the LED top surface flush with the casing (Figure 6a). This creates a smooth, continuous plane and shields the participant's fingers from the corners or edges of the LEDs **<C1>**.

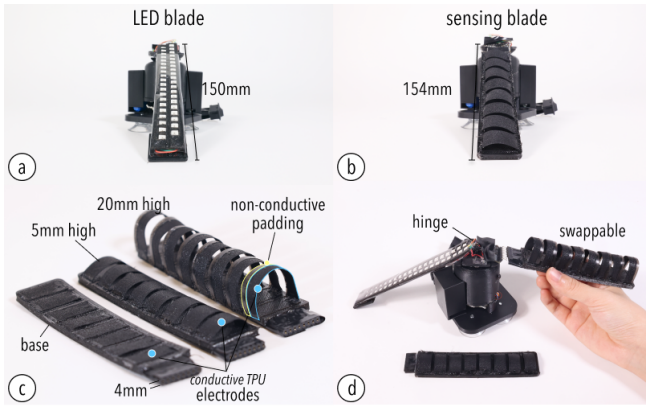


Figure 6: BloomBeacon uses a two-blade system: (a) an LED blade and (b) a sensing blade with soft electrodes. The sensing blade can have (c) various electrode heights. (d) The sensing blade is swappable.

3.4 Sensing Blade for Detecting Touch Inputs

One of our core contributions is centered around the sensing blade (Figure 6b). The sensing blade should invite touch and detect the user's touch location. The challenge the sensing blade is designed to address is to minimize the impact of touch disturbance **<C2>**, which is core to reliable display and sensing quality.

Safe and Stable Blade Base: At minimum, the sensing blade needs to be safe and comfortable to touch. We fabricated the blade base using a soft 3D-printable material, NinjaFlex TPU, similar to how this material is used to fabricate soft structures in elastic metamaterials [54]. We minimize the blade's weight by reducing the amount of infill to reduce the moment of inertia and thus the force on the user's finger. As our simplified physics model will show in Section 5.1, blade thickness is not an absolute metric as it interacts with other parameters such as weight and speed that collectively affect touch safety. Nonetheless, an ultra-thin base blade is undesirable for two reasons: (1) A thick edge reduces the pressure on the finger when fingers accidentally reach through the blades, making touch more comfortable and safe, and how the thickness value should be determined will be detailed in Section 5.1. (2) Thickness also helps the blade remain flat and stable while spinning, in contrast to a thin blade that easily flaps and twists while spinning and being touched.

The weight of the base blade is 10g, and we will show how weight and thickness affect safety in Section 5.1.

Electrode Design Minimizing Finger Disturbance: The goal is to only create physical contact during touch without stopping the rotation. To do so, we designed the electrodes to be soft, conductive arches. The arc shape deforms upon contact, providing a cushion between rotation and the finger, and giving the user a physical cue of when to stop. Before arriving at the current arc-shaped design, we also experimented with bristle-like electrodes, but they were too flexible and generated significant noise by contacting each other or being flapped by airflow during rotation. In contrast, the arc geometry balanced deformability and stability: it bends on touch yet remains steady while spinning. We also added non-conductive padding to electrodes to prevent neighboring conductive arches from touching each other (Figure 6c).

The electrode arches were fabricated with conductive TPU filament (Conductive Filaflex TPU) with a 0.2mm nozzle on a Bambu Lab A1 Mini printer. They were printed as 0.4mm-thick flat panels. By securing the two ends of the panel to the base blade using hot glue, the soft panels naturally formed arches. Longer panels result in taller electrode arches. We manually welded the wires to the conductive panels and routed them through the printed channels underneath the blade, connecting to the corresponding electrode on the capacitive sensor board. For the capacitive touch sensor, we use a low-cost, off-the-shelf, 8-channel CAP1188 sensor.

The sensor data is transmitted over the I2C bus through a slip ring to the microcontroller. I2C is susceptible to electrical noise. To reduce such noise, one hardware design was to make the motor and the MCU run on separate power lines and shorten I2C wires. This significantly mitigated the noise on the I2C bus caused by the current fluctuations from the motor.

The sensing blades in our implementation are designed to be swappable, as we discovered that different heights of the electrode arches offer different responsiveness and tactile sensations, which we will detail in later sections.

4 Sensing for Transient, Unstable Touches

One of the major challenges is to sense touch that is inherently brief and unstable **<C3>**. In this section, we discuss a series of optimization techniques centered around minimizing blocking and dealing with noise.

4.1 Minimizing Blocking in Software Design

The POV display places stringent demands on computing speed, and incorporating touch sensing further increases this load. It is critical that the program minimizes blocking during code execution (slowdowns that halt code execution until a task finishes). Capacitive touch boards, including the one we use, typically require brief sampling and sequential electrode scanning, which introduce delays that can disrupt display timing. To mitigate the effect, we employed a dual-core microcontroller so that the display and sensing can run in parallel. For our dual-core program, the primary core is dedicated to managing the LED display and the secondary core focuses on touch sensing. This prevents touch I/O from blocking the display timing. In addition, we configured the touch sensing task on the secondary core to have a priority level just below timer tasks. This ordering reduces preemption by less important processes and improves the responsiveness of touch sensing. We also adjusted the clock speed from the default 100 kHz to the fastest speed allowed (400 kHz) for touch sensor transactions to complete faster.

4.2 Touch Sensing Noise

Another major challenge was dealing with the noise generated during spinning. Here we illustrate the challenges and techniques we use to reduce noise. Note that the capacitive touch sensor we employ, CAP1188, is low-cost and off-the-shelf. The performance will likely improve with more advanced and custom sensors.

4.2.1 Electrode Calibration to Adjust Angular Offset. At 550 RPM, each revolution takes only about 0.11 seconds, meaning that rotation through each 2° slice of our device lasts roughly 605 microseconds. In our system, the sensor board supports eight electrodes where each electrode has varying latencies in response time. As each slice takes only a few hundred microseconds, these small per-electrode variations translate to different angular offsets that need to be corrected for each electrode. For example, as illustrated in Figure 7, there is an angular offset inherent to each electrode on the sensor board that needs to be calibrated. The electrode calibration process is elaborated in 5.2.1 and only needs to be done once.

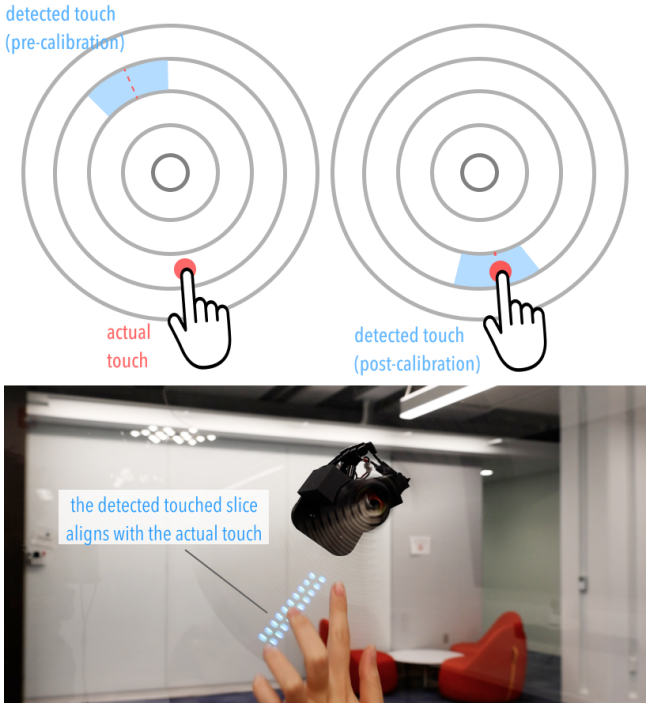


Figure 7: Calibration for each electrode to correct the angular offset, allowing the detected touch location to match with the actual touch location

4.2.2 Sensor Calibration during Motion. The spinning motion introduces significant noise. An effective technique to reduce such noise is to recalibrate the sensor after the rotation stabilizes and

before any touch. By doing so, the system learns a baseline that already accounts for the spinning state. In practice, we set the automatic recalibration to be 5 seconds after the device startup when the fan spins stably. This allows the device to treat the spinning as the background and make subsequent touch events distinguishable.

4.2.3 Touch Detection Window. Besides the noise that comes from the rotation, another source of noise comes from the touch itself, where false triggers come immediately after each touch event — even after the finger has left the electrode, the sensor board still registers touch events. This false detection might come from the deformation of soft electrodes or the slight disturbance of the rotation from the touch that just occurred. To tackle this, another critical feature we implemented is the touch detection window, which only registers the next touch after a six-revolution window has passed since the previous touch. This was effective in suppressing noise immediately after each touch event.

4.2.4 Software Tool for Specifying Interactive Areas. To make the interface customizable and usable across a variety of scenarios, we developed custom software to specify interactive areas as needed. As Figure 8 shows, one can do this by using our custom slicing software. The button area can be layered onto the sliced image. For example, a user interface consisting of two interactable buttons as shown in Figure 8 was used. After the image is loaded and processed into slices, the user can delineate button areas on the image. Our software allows the user to specify multiple buttons and outputs the slice and electrode ranges for every button accordingly.

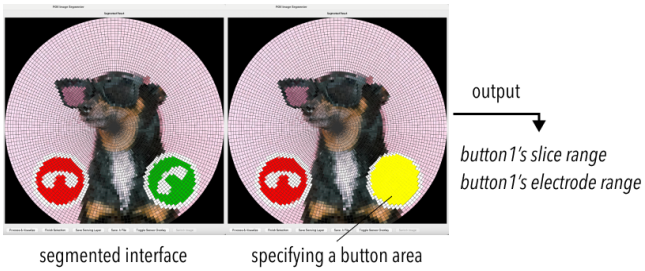


Figure 8: Button areas can be specified and exported with our custom software.

5 Technical Evaluation

In this section, we provide technical characterization to ensure safety with the blade design **<C1>**, together with investigating key factors that contribute to touch-sensing accuracy and touch response time.

5.1 Safety Characterization

5.1.1 Estimating Peak Contact Pressure. As we mentioned in Section 3, the blade causing cuts to the finger is one of the biggest safety concerns. However, this does not make such interaction infeasible; rather, it highlights the importance of tuning the relevant design parameters to enable safety. Below, we model and estimate the forces and pressures that may be applied to a finger based on the properties of the device (e.g., blade thickness/weight, rotation speed, etc.). While detailed finite element simulations may be needed to model the precise force between a soft edge and the skin, such approaches require material properties that may be difficult to measure for a quick safety assessment when deciding on the design. As a starting point, we adopt a simplified, well-established impact model from classical mechanics [11, 17]. It estimates the forces a rotating element produces at brief collisions. By plugging in easily measurable quantities, this model allows designers to decide key values to design for safety. More broadly, it can serve as a reference for other rotational systems that involve direct human touch.

5.1.2 Simplified Impact Model. We model the rotating element as a rigid body of known mass and geometry, with a compliant contact region (the soft blade edge and the fingertip) that determines the contact duration. The assumption for this simplified model is that during the brief impact, the motion of the rest of the device is not significantly altered, and the user's finger behaves as a passive compliant element.

The approach uses the concept of *effective mass* at the point of contact. For a slender strip of mass M and length L rotating about one end, the mass moment of inertia is

$$I = \frac{1}{3}ML^2,$$

and the *effective mass* at the tip radius, $r = L$, is

$$m_{\text{eff}} = \frac{I}{r^2} = \frac{M}{3}.$$

Given a rotational speed ω in radians per second, the tangential (tip) speed is simply

$$v = \omega r.$$

5.1.3 Time-Based Force and Pressure Estimation. We use the measured *contact time* t_c to capture the effect of both the TPU edge and finger compliance. For short impacts, the contact force often follows a half-sine pulse shape [17, 22], allowing the peak force to be estimated from the impulse–momentum relationship:

$$F_{\text{peak}} \approx \frac{\pi}{2} \cdot \frac{m_{\text{eff}}\, v}{t_c}. \tag{1}$$

Dividing by the contact area A yields the peak contact pressure:

$$P_{\text{peak}} = \frac{F_{\text{peak}}}{A}. \tag{2}$$

Equation 1 has a clear physical interpretation: for a fixed speed and mass, a longer contact time t_c directly reduces the peak force and pressure. A soft edge (e.g., TPU85A) increases t_c, thereby lowering the peak force.

5.1.4 Peak Force and Pressure Estimation for the Implemented Device. We apply the parameters of our implemented device to demonstrate the model and validate the contact safety for our system. We measured the key parameters of our prototype:

- Rotational speed: 550 rpm $\Rightarrow$ $\omega = 58.0$ rad/s
- Strike radius: $r = 0.154$ m
- Tip speed: $v = 8.93$ m/s
- Mass: $M = 0.011$ kg $\Rightarrow$ $m_{\text{eff}} \approx 3.67 \times 10^{-3}$ kg
- Edge contact area (using an estimated finger size): thickness 4 mm$\times$ finger width 15 mm $\Rightarrow$ $A = 6.0 \times 10^{-5}$ m^2

The last parameter is the contact time t_c, which can be measured by taking slow-motion videos on a camera or a force or torque sensor. We measure t_c using a torque sensor (ATO Flange to Square Drive Reaction Torque Sensor) by letting the fan blade hit the edge of the sensor attachment (Figure 9). By sampling the torque sensor reading, we can get the contact time by checking the duration of the torque spikes. We repeated the contact time measurement ten times. The average contact time is 40 milliseconds. Using Equation 1 and plugging in t_c, we have the estimated peak force and pressure shown in Table 1.

t_c (ms)	F_{peak} (N)	P_{peak} (MPa)
40	1.29	0.0214

Table 1: Estimated peak force and pressure from measured contact time

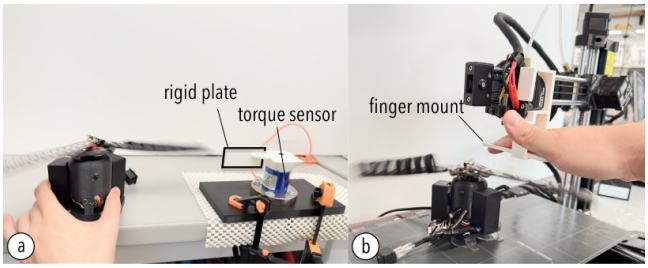


Figure 9: (a) Contact time and estimated force measurement using a torque sensor. (b) Touch-sensing accuracy evaluation using a modified 3D printer

5.1.5 Experiments. We performed experiments to verify our estimated force using the torque sensor mentioned above. The force is calculated by dividing the measured torque by the length of the attachment arm. The average actual F_{peak} from ten measurements is 1.01 N, which is slightly below the estimated force of 1.29 N. The pressure P_{peak} based on the measured force is 0.017 MPa, below the estimated pressure of 0.021 MPa, likely because our equation holds a conservative assumption that the motion of the rest of the blade is not significantly changed, while the contact actually caused more bending and deformation of the elastic blade.

Prior experimental studies have reported that the stresses required to initiate cutting in soft biological tissues such as gelatin and human skin are typically in the range of 0.1–1 MPa [9, 18, 47]. This range provides a useful benchmark for interpreting our estimates of peak contact pressure, and both the estimated (0.021 MPa) and measured values (0.017 MPa) are significantly below the lower bound of the benchmark (0.1 MPa). Our simplified model shows that the peak force depends directly on both the effective mass and velocity of the rotating blades, and inversely on the contact duration. This has clear design implications: while increasing speed or mass increases the potential for harmful contact, prolonging the contact duration through softer edge materials or more flexible geometries effectively reduces the peak force. We acknowledge that the dynamics between motion, material properties, and finger contact involve a far broader set of parameters than those examined here. Future work should investigate these dynamics in greater depth (for example, modeling edge buckling behavior [9]) to fully understand the parameters that affect safety and comfort. Our simplified model is intended as an initial reference point to offer designers a framework for reasoning about safety and comfort and for tuning major aspects of the design.

Although our modeling focuses on avoiding cuts, other safety-oriented designs should also be considered. Ensuring that fabrication processes in reality produce smooth surfaces as intended is essential to avoid scratches. Entanglement with loose items such as hair is another concern. To address this, we implemented an auto-stall mechanism that detects weak external resistance and stops the motor (Section 9.1.1).

5.2 Touch Sensing Accuracy

As an initial exploration into allowing the spinning, soft assembly to support touch sensing, we examine whether and how *rotation speed* and *electrode height* affect sensing performance. While Section 7 reports a user study evaluating the system's end-to-end performance, here we focus on characterizing touch-sensing accuracy under controlled conditions.

Before identifying the configurations that yield the most accurate results, a more fundamental question is whether speed and electrode height affect different aspects of performance. Studying this can offer future researchers and engineers generalizable insights into which parameters can be optimized for what purpose, even if different materials or components are adopted. Therefore, we measure and present data across three rotation speeds and three electrode heights. We also report outcomes from less optimal conditions to provide a full comparison across the tested parameters.

5.2.1 Procedure. Our blade contains eight electrodes, corresponding to the eight channels our capacitive sensing board provides. All electrodes on each blade were tested under three varying speeds of 350, 450, and 550 RPM and three varying heights (flat, medium, and high electrodes, as shown in Figure 6c).

We use a 3D printer to move a finger held in place up and down to repeatedly make contact with the same location and height on each electrode. The detected touch slice and electrode were recorded. With highly controlled touches, this evaluation focuses on the system itself, disregarding user touch variability.

Using the open-source software OctoPrint, custom G-code was used to move the mount up and down to repeatedly move the finger and touch each electrode. A mount was created for a Prusa Mini+ 3D printer in order to hold a finger in place while it was moved up and down. The mount is designed to allow a user to insert their index finger and position it such that the pad of the finger is exposed through a hole, while the rest of the finger is held rigid.

The finger touches the 0-slice position shown on the display. Fifty touch inputs were collected for each condition listed above and saved for analysis. We also use this data for electrode calibration as mentioned in Section 4.2.1.

5.2.2 Angular Accuracy. We present the angular accuracy of our system using circular STD, which quantifies the spread of the angular data [12]. Unlike linear statistics, circular statistics explicitly

account for the nature of angular data, where high and low values wrap around (e.g., 359° is adjacent to 0°) and the zero degree is arbitrary. In this context, measures such as variance or standard deviation on a linear scale would give misleading results. Circular STD provides an established metric for describing how tightly touch interactions are distributed around a target angle, making it well-suited for evaluating the angular accuracy of our system. The reported results should be seen as a baseline, since faster and more capable sensors could further improve the angular spread.

Speed Effects. Figure 10 top illustrates the circular STD across eight electrodes for three rotation speeds (350, 450, and 550 RPM) on the same mid-height blade. Each blue arc represents the double of the circular STD to reflect ±STD. One-way repeated-measures ANOVA (after normality validation) revealed **a significant effect of RPM on angular spread** ($F(2, 14) = 4.514$, $p = 0.031$).

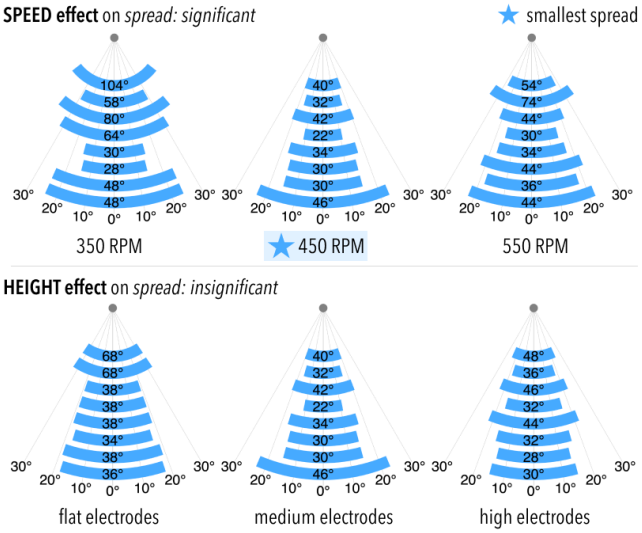


Figure 10: Circular STD data. The angle of each blue arc is 2 × CircularSTD. Top: circular STDs under 350, 450, 550 RPM. Bottom: circular STDs of flat, medium, and high electrodes. Speed has a significant effect on spread, and 450 RPM shows minimal spread. Height effect on spread is insignificant under controlled touches.

Height Effects. Figure 10 Bottom shows the angular spreads for three electrode heights (flat, medium, and high). Shapiro–Wilk normality test revealed normality violation in the flat condition, thus we conducted a Friedman test, which did not show a significant effect of the height on angular spread ($Q = 4.0$, $p = 0.14$).

5.3 Touch Response Time

We report the system touch response time from the onset of touch to the illumination of LEDs. This allows us to characterize the system's latencies, especially given the transient detection window, and investigate whether and how configuring electrode heights and rotation speeds can reduce latencies.

5.3.1 Procedure. Touch input was repeated on each electrode for 10 detections, resulting in 80 valid touches per blade. An LED ring illuminated upon touch detection. A trial was considered valid if the system detected the touch within 5s. If no detection occurred within 5s, the trial was recorded as a detection failure. The 5s duration is intentionally lengthy to serve as a conservative cutoff, since a successful detection usually occurs immediately after touch rather than after a few seconds' wait, as we will show in Results.

Response time was measured from slow-motion videos recorded at 240 fps, which produces one frame about every 0.004s, yielding a negligible measurement error of 0.4–0.7% relative to our measured latencies. Both the finger contact and the onset of LED illumination were clearly identifiable from the recording. To investigate whether rotation speed and electrode heights affect the system's touch response time, we again repeated this test for 350, 450, and 550 RPM for the speed condition, and flat, medium, and high electrodes for the height condition to elicit learnings for the conditions with the fastest touch response.

5.3.2 Results. Across rotation speeds, average response time ranged from 0.53s (550 RPM) to 0.85s (450 RPM), as shown in Figure 11, though the error bars indicate substantial variability.

Across electrode heights, average response time ranged from 0.65 s (high electrodes) to 0.93 s (flat electrodes). Flat electrodes also showed the greatest variability. Within the heights tested, higher electrodes support more robust and responsive touch.

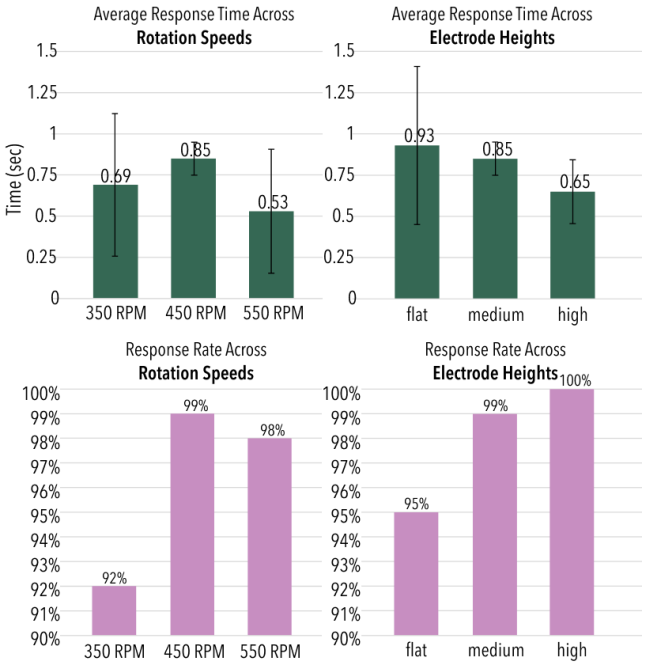


Figure 11: Top: Average response time across rotation speeds and electrode heights. Bottom: Touch response rate across rotation speeds and electrode heights.

Most touches were detected. We would also like to report the occasional detection failures, where touch detection did not happen within 5s. In Figure 11 Bottom, across rotation speeds, the lowest rate occurred at 350 RPM (92%), whereas 450 and 550 RPM showed

higher rates (99% and 98%, respectively). One possible reason for the lower response rate at the slowest speed may lie in our *hinged* blade design. The hinge prioritizes safety by allowing the blade to lower upon touch. At slower speeds, the reduced moment of inertia makes it harder for the blade to maintain its height, which may decrease the contact stability.

Across electrode heights, response rates increased with height: flat: 95%; medium: 99%, and high: 100%. Although response performance was strong across all electrode heights, higher electrodes yielded the most reliable results (100%).

6 User Study

As BloomBeacon is a novel type of interactive hardware that is unconventional to touch, we conducted a user study to validate the interaction with our proof-of-concept device, and extracted insights from user interaction and responses. Specifically, the study characterized and evaluated BloomBeacon's end-to-end performance for touch display interaction and user experience. We ask three questions — Q1: How do users perceive and feel about touching a POV display, based on our implementation? Q2: How do speeds and heights affect user touch accuracy and user experience on both the angular and radial axes? Q3: How do participants feel about performing conventional touchscreen gestures (tapping, holding, sliding, zooming in/out) and other gestures unconventional for touchscreens (petting, scratching, and light punching)? We will answer Q1 with 7-point ratings for different speed and height conditions and qualitative interviews. We will report quantitative user touch data and qualitative feedback for Q2, aiming to understand the impact from different parameters and to identify the best conditions. Lastly, we will share participants' ratings on performing the aforementioned gestures on BloomBeacon for Q3.

6.1 Participants

We recruited 10 participants (5 male, 5 female; all right-handed). Our participants' ages range from 21 to 65 (M=29, SD=13). Individuals were excluded if they self-reported photosensitive epilepsy, anxiety or sensory processing disorders, or any physical impairment that would prevent interaction with touch screens. The setup is shown in Figure 9. All study sessions took place in the same conference room in our institution with the same lighting conditions. The lighting was bright, with a brightness of 914 lux measured by the Light Meter app on an iPhone 14 Pro. We kept the room lighting consistent across the study sessions.

6.2 Procedure

Before and after the researcher demonstrated the touch interaction, participants were asked to share their comfort levels with touching the spinning device. After this introduction, we proceeded to the two primary tasks. Task 1: A targeted touch task that measured the range of user touches on both angular and radial axes under 3 speed conditions and 3 blade height conditions (about 40 min). Task 2: Gesture preferences on different blade heights (about 20 min). Before Task 1 started, we let each participant perform a practice round to get familiar with tapping the spinning display. They were allowed to proceed to the main task when they felt comfortable. Most were able to proceed within 10 minutes.

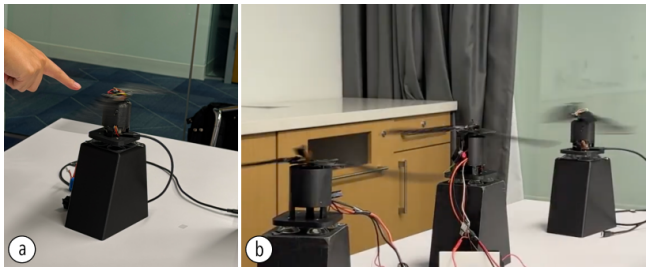


Figure 12: (a) The setup for the targeted touch task. (b) The setup for gesture exploration.

The study was approved by our institution's IRB office (IRB number: IRB25-1247), and participants were compensated with a $20 Amazon gift card. Each session took about one hour.

6.3 Task 1: Targeted Touch

The targeted touch task is to tap a sequence of dots that show up on the display, as shown in Figure 13b. The 16 targets are as shown in Figure 13a, covering 4 angles, 4 electrodes, 4 repetitions, resulting in 64 trials for each condition. Each participant received a random order of 64 targets. When a tap is successful, the outer edge of the display will light up green (Figure 13c), forming a green ring to inform users of the completion of a touch, and a new dot will appear. We randomized the order of the targets for each participant. We asked that the participant touch a target as soon as they see it, and touch nowhere else on the display to prevent unintended touch inputs. Considering participant fatigue, we only tested four electrodes (0, 2, 4, 6, as in Figure 13) out of eight. Participants were only allowed to use one finger to perform the touch.

There were three speed conditions (350, 450, 550 RPM) and three blade electrode height conditions (0mm, 5mm, 20mm) — a total of 320 trials per participant to examine the effects of speed and electrode height. The orderings of the speeds and electrode heights were randomized to compensate for fatigue and order effects.

The detected touched slice and electrode were logged for every touch event along with the target slice and electrode for that touch. The total time for completing all targets was also logged once the participant finished the last target.

After each speed-height combination, participants were asked to rate their experience on a scale of 1 to 7 for the following questions: (1) *How responsive do you think the display is?* (2) *How comfortable did you feel while touching?* (3) *How confident were you about when and where to touch?* (4) *How enjoyable or fun was the experience?*

6.4 Task 2: Performing Different Gestures on Different Electrode Heights

The input blades with non-flat electrodes essentially introduce softness and depth to the touch display. Therefore, we explored what type of gestures this depth enables or enhances.

As shown in Figure 12, the three devices mounted with blades with flat, medium, and high electrodes will spin together. The position ordering of the blades was randomized for participants. We asked participants to perform a specific gesture from left to right sequentially first, and then they were allowed to freely try all devices.

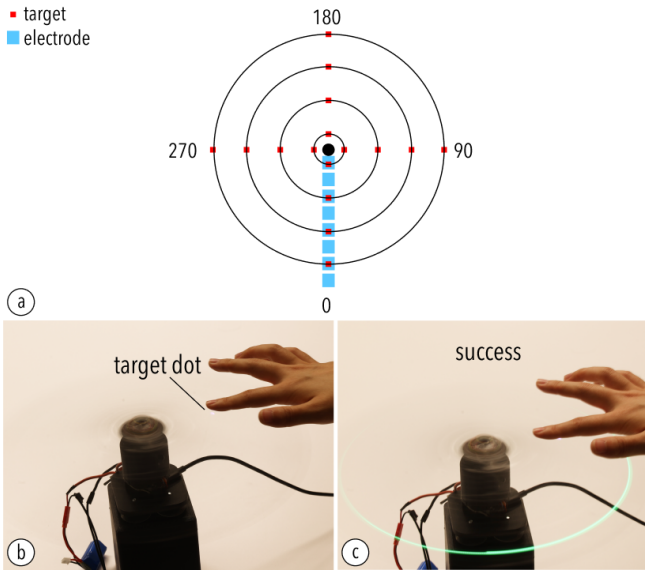


Figure 13: (a) Target dot positions. (b) A target dot on the display. Note that the target dot is more visible in real life than in the photo. (c) The touch success indicator.

Note that there is no sensing or gesture recognition involved for gesture exploration; our goal is to first understand user experiences and preferences prior to future implementations.

We asked participants to perform conventional touchscreen gestures, including tapping, holding, sliding, zooming in and out. Since our electrodes are soft, we also wanted to explore gestures that are unconventional for touchscreens but common for soft surfaces, such as scratching, petting, and punching. We demonstrated to the participants the exact gestures as shown in Figure 14.

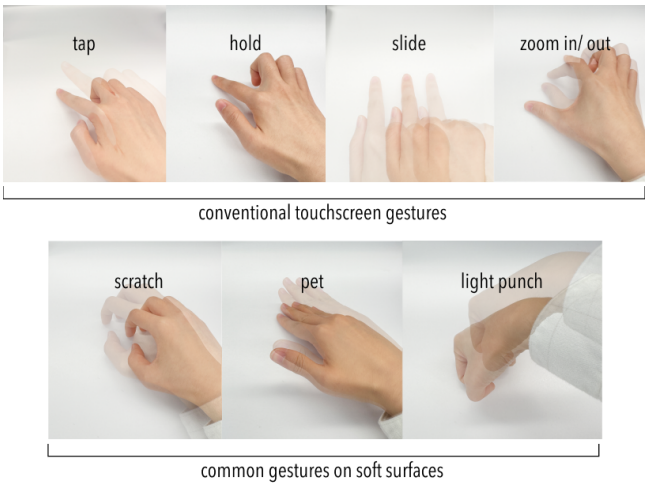


Figure 14: Gestures participants were asked to perform.

For each gesture, the participant was asked to rate from 1 to 7 on how comfortable they are performing the gesture on each electrode height and how performing that gesture on our display differs from performing it on a regular touchscreen.

7 User Study Results

In the following sections, we present results to answer the three research questions in Section 6. The results presented in this section reflect performance across all three speeds (350, 450, 550 RPM) and three electrode heights (flat, medium, high). Unlike the in-lab technical evaluation with highly controlled touches, the results from the end-to-end user study can help us understand how speed and height affect touch experience and accuracy under realistic and varied user touch styles.

Results from all conditions will be reported and compared, including both the best and worst ones, to reveal the impact of touches on rotation under different conditions. This corresponds to one of the core challenges we identified in POV-based touch displays **<C2>**. We will draw insights from these results and recommend conditions that yield the best result.

7.1 Participants' Initial Comfort Levels

For the comfort-level question, we asked the participants to touch and explore the device in the beginning when it was not yet spinning. Participants described the blade material as *"soft"* (P4, 6, 7, 8, 9), *"spongey"* (P10), *"rubber"* (P2, P6), and *"bendable"* (P3). When they first saw the device spinning, their average comfort level with touching was $M = 4$, $SD = 1.63$. After the researcher demonstrated touching, their average comfort level rose to $M = 6.3$, $SD = 0.67$.

The initial discomfort and improved comfort after watching imply that the device may be better suited for personal use in familiar environments, such as personal space, rather than as a walk-up-and-use system in public spaces.

7.2 Results for Task 1: Targeted Touch

Our 10 participants produced 3200 tap trials for this task that characterize the end-to-end accuracy of targeted touch. As our angular data was circular, we did not remove any outliers.

7.2.1 Average Trial Length. For each participant, we measured the total duration to complete 64 trials and calculated the average trial length. While the system response time was measured in Section 5.3.2, the average trial length (Figure 15) measures the end-to-end time, including locating the target, reaching toward it, and the system response. Among the three speeds, the fastest 550 RPM speed had the shortest duration (2.3s). Among the three heights, the shortest is from the high electrodes, only about 60% of the duration of the other two. The trend for both speed and height largely aligns with the system response time measured in Section 5.3.2. From our observation and interview, participants tapped more quickly and with less care on high electrodes: *"the [high] blade made more contact"* (P8); *"the most responsive of all"* (P5); *"not needing to touch the blade itself... No need to think about finger depth"* (P9).

7.2.2 Angular Accuracy. While Section 5 characterizes the angular accuracy of a consistent spot being repeatedly touched, here we report the combined error of both the system and the participant. We identified three major sources of error: 1) the system's inaccuracy, including limitations of the sensor board and the fabrication quality

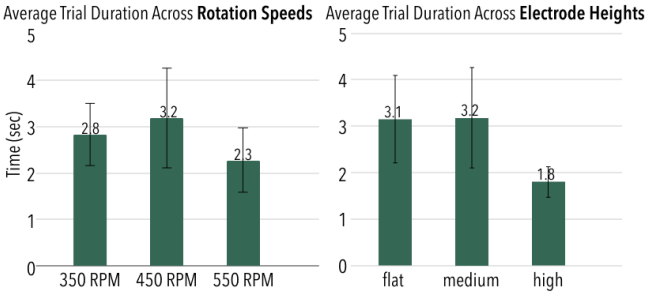


Figure 15: Average trial length (including locating the target, reaching toward it, and the system response): (a) across different rotation speeds; (b) across different electrode heights

of the conductive electrodes, 2) users' touch inaccuracy, especially given the target dot appears floating in the air, 3) disturbance of rotation speeds due to touching.

We report how speeds and electrode heights affect spread in Figure 16 and angular offset in Figure 17. As in our technical evaluation, spread is circular STD; angular offset reflects a systematic shift of the circular mean. Although the target electrodes were limited to 0, 2, 4, 6, participants also touched nearby electrodes such as 1, 3, 5, 7; thus, our angular results cover all eight electrodes. Our user study data illustrates the end-to-end touch accuracy, accumulating system performance, varied user touch styles, and user errors.

Speed effects. We will analyze speed effects on touch spreads and offsets separately below.

Spread: Figure 16 top shows a spread-only visualization. The blue arc shows 2 × CircularSTD to represent ±CircularSTD. One-way repeated-measures ANOVA (after normality validation) revealed **a significant effect of speed on angular spread** ($F(2, 14) = 5.383$, $p = 0.018$). Post-hoc paired t-test (Bonferroni-corrected) showed significant comparisons: 350 vs. 450 RPM ($t = 3.2$, $p = 0.047$); 350 vs. 450 RPM ($t = 3.14$, $p = 0.049$); 450 vs 550 RPM ($t = 1.131$, $p = 0.885$). **350 RPM shows the smallest spread** while there is no significant difference between 450 and 550 RPM.

Offset: Figure 17 Top shows the angular accuracy for 350, 450, and 550 RPM with the mid-height electrodes. The red center line represents the angular offset of each electrode compared to the zero-degree centerlines. Offsets were near zero on average, with positive deviation at 450 RPM ($M = 8.5°$, $SD = 11.9°$), small positive deviation at 350 RPM ($M = 3.1°$, $SD = 10.5°$), and a slight negative deviation at 550 RPM ($M = -2.1°$, $SD = 9.6°$). These offsets can be easily added to the code for systemic correction. The Shapiro–Wilk test revealed normality violation in medium conditions, thus we conducted a Friedman test, which did not show a significant effect on speed ($Q = 4.8$, $p = 0.09$).

Another overarching observation is that the outermost electrodes tend to yield more offsets and spreads. We attribute this to three factors — First, the outer electrodes rotate at a larger radius and therefore higher linear speed, which makes them more difficult to activate and less responsive compared to the inner areas (P4, P6). Second, as participants tried harder at the periphery, they tended to disturb the rotation more, causing more inconsistency in motor speeds (P1, 2, 9). We also observed occasional accidental contact

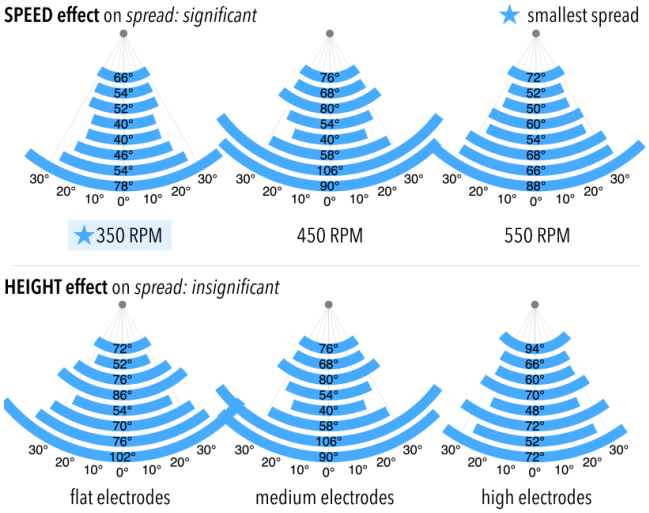


Figure 16: A spread-only visualization. Speed has a significant effect on spread. Among the conditions, 350 RPM shows the minimal spread. The height effect is insignificant.

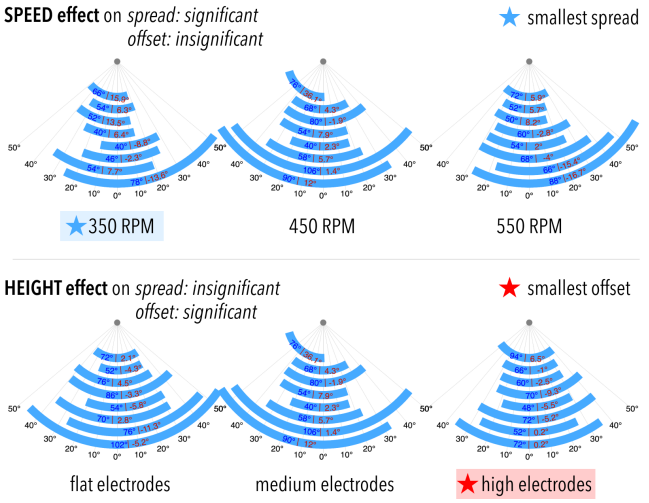


Figure 17: A spread and offset visualization. Offset: Height has a significant effect on offset. The high electrodes (red-starred) yield the smallest offset. Spread: See Figure 16 for a cleaner spread visualization and analysis.

with participants' elbows when they reached toward the inner electrodes, which may have triggered unintended touch location at the periphery to some extent.

About user experience, some participants prefer slower speeds: *"[slowness] helped with comfort"* (P1) and *"makes it easier to touch"* (P9). However, some participants *"had to press lower or a bit more on slow speed"* (P5). The slowness also affects the display quality, the slow speed made the display *"flickered more"* (P7).

Height effects. We report the analysis for electrode height effects on spread and offset below.

Spread: Figure 16 Bottom shows a spread-only visualization. A repeated-measures ANOVA showed no significant effect of electrode height on angular spread ($F(2, 14) = 0.434$, $p = 0.656$). This aligns with the finding from Section 5.

Offset: Figure 17 bottom shows the height effect on offsets. Offsets were close to zero at the flat ($M = -2.6°$, $SD = 5.3°$) and high ($M = -2.1°$, $SD = 4.8°$) heights, but positive at the medium height ($M = 8.5°$, $SD = 11.9°$). The Shapiro–Wilk normality test revealed normality violation in the medium condition, thus we conducted a Friedman test, which showed **a significant effect of height on offset** ($Q = 9.250$, $p = 0.010$). Post-hoc Wilcoxon signed-rank (Bonferroni-corrected) showed significant comparisons: low vs. medium ($W = 2.0$, $p = 0.07$); low vs. high ($W = 18.0$, $p = 1.00$); medium vs. high ($W = 0.0$, $p = 0.02$). **Overall, high electrodes are recommended for the least amount of offset.**

Experience-wise, most participants favored the highest electrodes (20*mm* high): *"significantly more comfortable"* (P6); *"enjoyed the texture the most... the touch of the material was fun... the softness was very comfortable"* (P7); *"the most comfortable because of the softness"* (P9); *"less fear, the most fun, like flapping wings"* (P3).

The flat blade received the most negative feedback, possibly because the risk of disturbing the rotation is higher, and the touches need to be more careful: *"felt it hit harder when the finger made contact with the blade"* (P7); *"comparatively less comfortable"* (P10); *"significantly less responsive"* (P4).

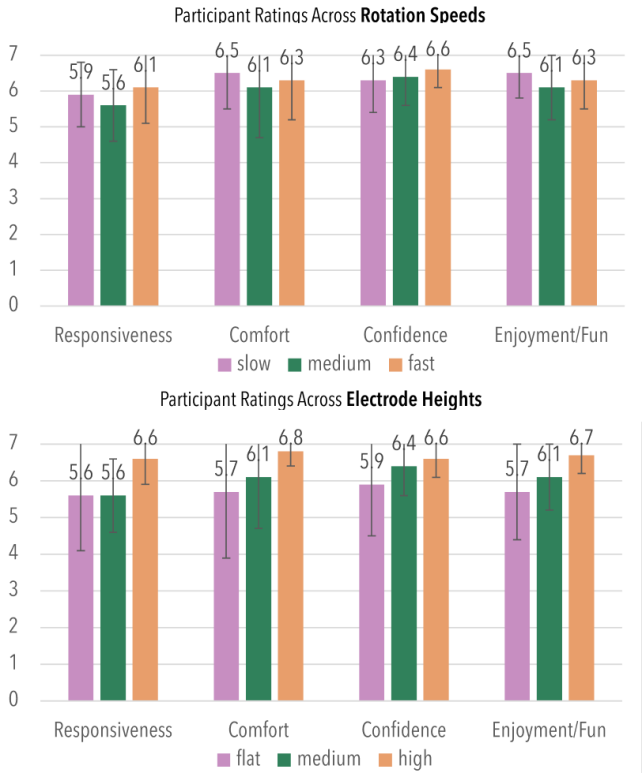


Figure 18: Participant ratings on responsiveness, comfort, confidence, enjoyment across different speed and height conditions

7.2.3 Radial Accuracy. The radial axis corresponds to the direction along which the electrodes are aligned. The radial positions of the target dots were mapped to be the center of the target electrodes 0, 2, 4, 6, where 0 is the closest to the center. Each electrode is 10mm long on the radial axis with 5mm spacing in between electrodes, which defines the radial resolution of our current blade design.

Figure 19 shows the confusion matrix between target electrodes and touched electrodes. This matrix includes all speeds and height conditions. The diagonal cells represent correct touches, while the off-diagonal cells indicate mistouches. We can see that most mistouches occur within ±1 electrode around the target. With our current radial resolution, this means a ±15*mm* range from the target location on the radial axis. Note that there are quite a few mistouches from the outermost electrodes, likely due to the mistouches from participants' elbows when they tried to reach inside.

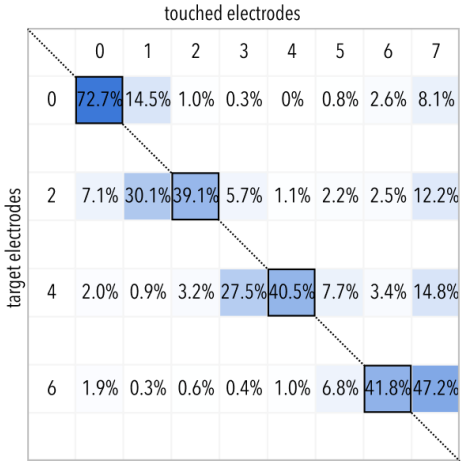


Figure 19: Confusion Matrix of Target vs. Touched Electrodes for all speed and height conditions

Speed Effects. Figure 20 Top shows confusion matrices among 350, 450, 550 RPM. Across all speeds, the innermost electrode has the highest accuracy, partially because it has only one adjacent electrode. A consistent pattern emerges for electrodes in the middle region (e.g., 2 and 4): mistouches tend to drift inward toward the center. In contrast, electrodes closer to the outer edge (e.g., electrode 6) show more frequent mistouches outward to electrode 7 at the edge. This indicates different mistouch tendencies depending on an electrode's distance from the edge.

Height Effects. Figure 20 Bottom shows confusion matrices for different electrode height conditions. Most of the patterns observed in the speed conditions also apply here. Besides, higher electrodes show improved accuracy for electrodes 2 and 4 compared to the other two heights, but worse accuracy for electrode 6 at the edge.

7.3 Results for Task 2: Experience of Performing Different Touch Gestures

We report participants' ratings and responses about performing conventional touchscreen gestures (tapping, holding, sliding, zooming in/out) and other gestures unconventional for touchscreens (petting, scratching, and light punching) on our display.

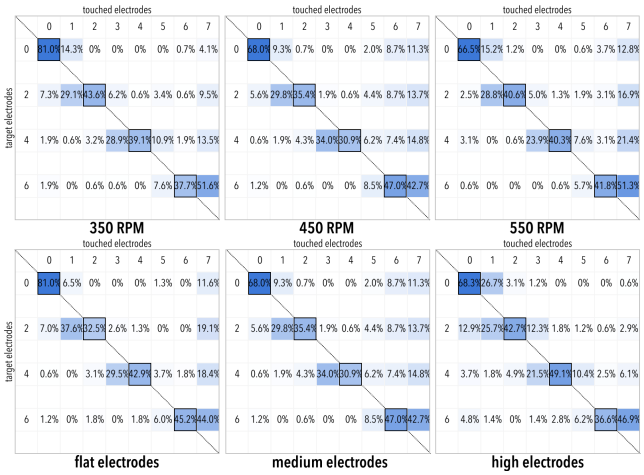


Figure 20: Target vs. Touched Electrode Confusion Matrices

Among all interactions, the high electrode height is favored overall. Among the four conventional touchscreen gestures — tapping, holding, sliding, and zooming in and out — tapping and holding received the highest comfort ratings, likely because they are the simplest and have been extensively practiced via the previous task.

Zooming in/out has the lowest average score. The interview revealed a lack of perceived controllability: *"Sometimes [the feedback] goes away, sometimes it comes"* (P3). *"Feel like jumping a bit, not continuous"* (P5); *"feel a bit in the air"* (P8); *"disconnectedness"* (P10). This issue was most pronounced during gestures requiring continuous contact, like sliding and zooming, which may not be well-suited for this type of display.

Finally, we are particularly interested in the user experience of gestures that are common for soft textures: scratching, petting, and light punching. Participants enjoyed that the high soft electrodes support these gestures being performed with depth: *"[scratching] is a great gesture for these machines. The spinning makes the gesture more feedback to the user."* (P9); *"The depth allows the curve movement of petting."* (P7). *"I'd rather do petting on this [high electrodes] compared to a regular touch screen"* (P2); *"It feels comforting, light, gentle. There is a rhythm. Petting a touch screen does nothing; [the high blade] is nice"* (P5); *"It would hurt a lot more if I punched my phone screen... more abrasive on the knuckles."* (P10); *"[Punch] feels very padded, feels very comfortable."* (P1).

However, there is also a general concern of disturbing the rotation if the gesture is performed too strongly: *"Need to be mindful of the depth"* (P5). While some participants enjoyed the feedback, several participants thought the feedback was too much. *"although it's not hitting, I'm interrupting too many things"* (P9) *"I feel I moved with the screen... need to find the balance between what I do and [what] the device will do."* (P6)

Overall, the softness and depth of the electrodes can potentially inspire more diverse tangible interactions with graphical contents.

7.4 Result Discussion and UI Implications

In summary, high electrodes had the shortest system response time and total interaction time. *Spread* is significantly affected by speed; the slowest speed was the best. *Offset* is significantly affected by electrode height; the highest electrode was the best. Taken together, high electrodes at slow speeds should produce the best overall angular accuracy. On the radial axis, the spread is fairly consistent across all conditions. User-experience-wise, high electrodes were favored overall.

The results also have implications for UI design. We propose the following layout suggestions to minimize the effect of angular inaccuracy. For example, in Figure 23, the first UI is not recommended because all three buttons A, B, and C are on electrode 2 (the grey ring), which makes angular accuracy the sole determining factor. Alternatively, Layout 1 places button B on a different electrode (the yellow ring) while A and C are distant angularly, reducing the reliance on angular precision. Another layout, Layout 2, allows a straight placement of three buttons, each on a different electrode. In general, it is recommended that layouts avoid clustering multiple buttons on the same electrode and instead spread buttons across different angular and radial positions.

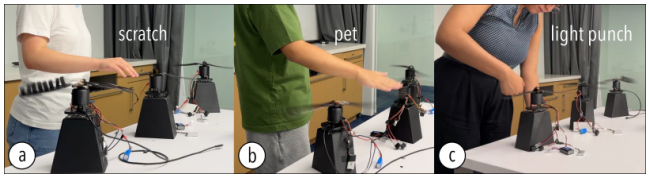


Figure 21: From the gesture exploration in the user study: (a) scratch, (b) pet, (c) light punch.

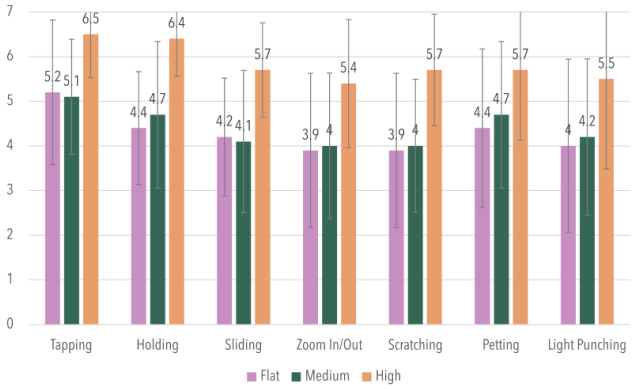


Figure 22: Participant ratings on different gestures

8 Application Examples

In this section, we present four applications that demonstrate various dimensions of BloomBeacon. As a physical display itself, we show its tactile potential in supporting soft surface interactions. When in the environment, we highlight its potential to be easily placed to flexibly augment physical objects and devices.

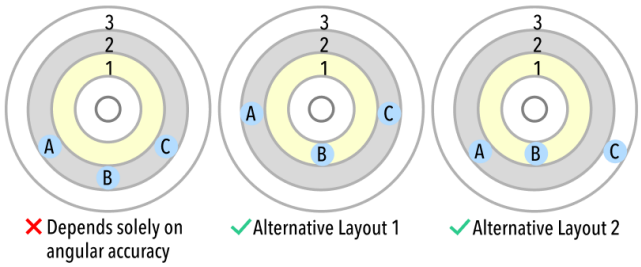


Figure 23: UI layout suggestions

8.1 Soft Surface Interactions

Our display's blooming soft surface enables graphical content to be experienced with a tactile quality, offering soft textures that traditional rigid screens struggle to convey. The high, soft electrodes further introduce a sense of depth, enhancing the three-dimensionality of the interaction. As shown in Figure 24, the display renders a furry dog, and users interact with the soft electrodes in a manner reminiscent of petting the dog's fur. Other tactile sensations could be explored by swapping in the blades of different heights or softness.

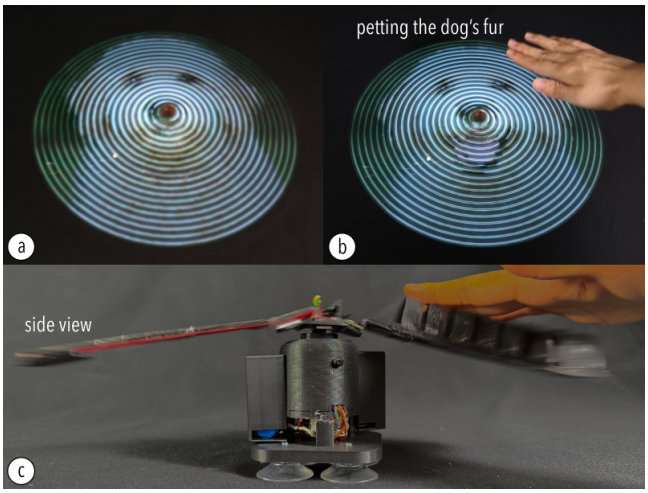


Figure 24: (a) The display of a furry dog. (b) The user pets the dog and experiences a soft sensation, while the tactile feedback is provided by the (c) high, soft electrodes.

8.2 Augmenting Physical Objects and Devices with Limited Space

BloomBeacon's ability to bloom from a compact form allows it to augment objects with limited surface area that cannot accommodate a built-in screen.

As illustrated in Figure 25, a user places BloomBeacon on a small speaker. The device displays the album art for the current song and allows the user to change tracks by touching graphical buttons on its surface. In this example, a speaker with only basic buttons can be enhanced to display the album art of the current music, offering rich visual information similar to what a phone music player can provide. This allows for a temporary extension of an object's functionality and interactivity, creating an on-demand touch display without altering the object's original form.

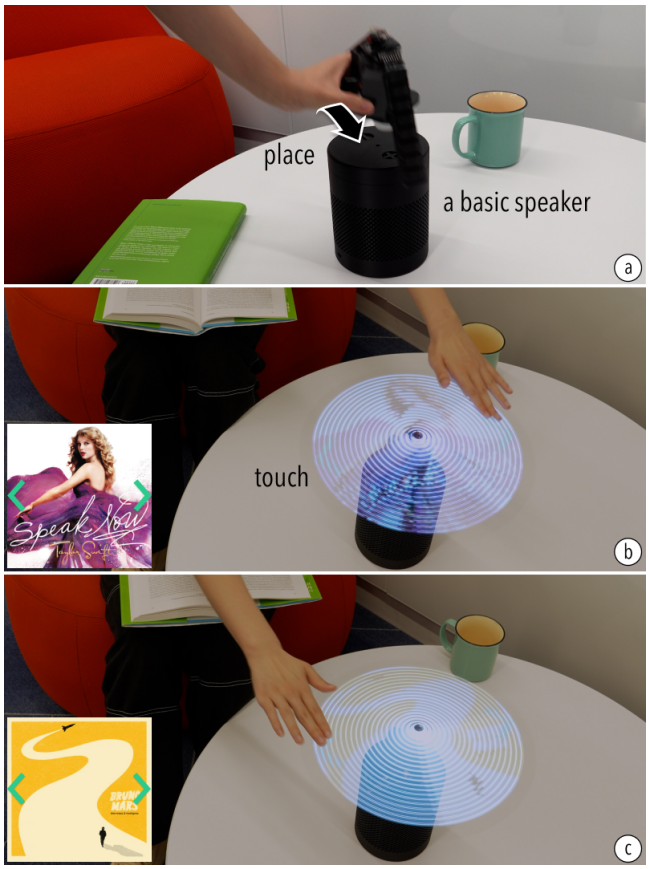


Figure 25: (a) The user places BloomBeacon on a speaker ad-hoc. (b) BloomBeacon displays the album art for the song that is playing on the speaker. (c) Touching the buttons on the display allows the user to change songs.

8.3 Pop-up Mid-Air Displays

The line-like form factor makes it easy to store along linear elements, such as the edge of a shelf, while only blooming into a large mid-air surface when needed. For example, Figure 26 illustrates that when a user attempts to reach for a hazardous chemical bottle without gloves, the device blooms into a physical surface that blocks access. The display shows a warning prompt and a confirmation button. Once the user presses the button to acknowledge the requirement, the spinning motion stops and the display surface disappears, allowing the hand to reach inside.

8.4 Overlaying Graphical Content on Physical Environments

We augmented a paper map by overlaying interactive weather information, as shown in Figure 27. The graspable, modular device form factor allows it to be easily moved to different regions on the map to

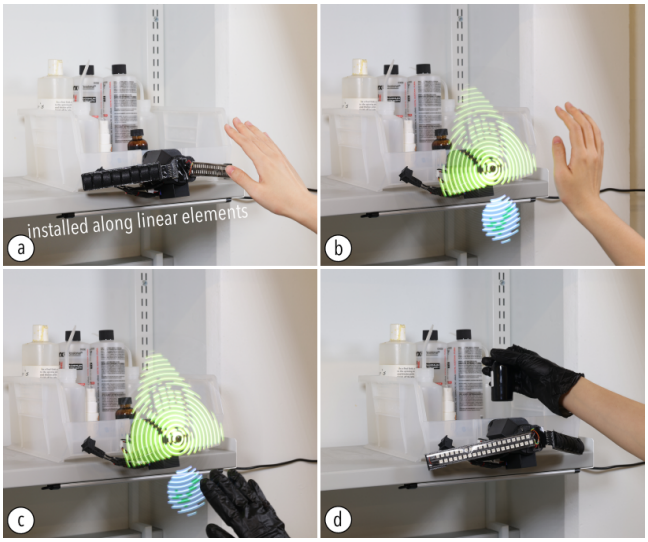


Figure 26: (a) The user reaches for a chemical solution without wearing protective gloves. (b) BloomBeacon blooms into a surface, blocking the hand and displaying a warning. (c) The user puts on gloves and confirms the action on the touch display. (d) The device stops spinning and the surface disappears, allowing the user to reach in.

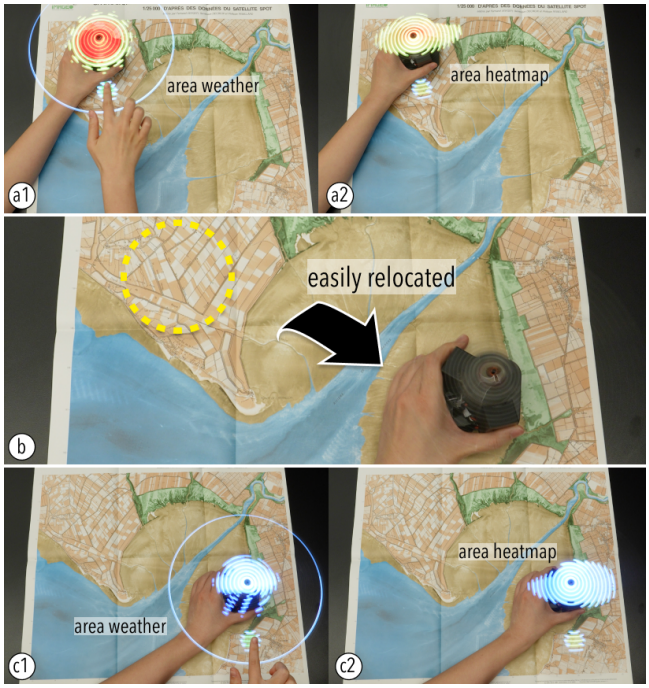


Figure 27: On a paper map, (a1) BloomBeacon shows that the region the device covers is sunny. (a2) Upon a button press, the interface changes to overlay a heatmap of the region. (b) BloomBeacon is then moved to a different region where the weather is rainy. (c1-c2) A button press can switch between weather and a heatmap.

show the local weather. The touch display shows a button, allowing to switch to a heat map. This application demonstrates BloomBeacon's potential for blending digital information and interaction into the physical environment in a direct, tangible way.

9 Discussion, Limitations, and Future Work

In this paper, we presented the concept of blooming a touch display via Persistence-of-Vision motion. We identified and structured the core challenges of POV-based touch and demonstrated our initial solutions through a proof-of-concept implementation that encompasses device mobility, safety, sensing, and user experience. As the first work to articulate and tackle these challenges, our contribution is foundational rather than exhaustive. In this section, we present additional features and supplementary experiments that further address these broader considerations. We will also discuss the limitations of our current prototype and share lessons we learned from our development process with fellow researchers. Lastly, we will point to some exciting future research directions.

9.1 Additional Safety Features

9.1.1 Automatic Stall Detection. While our simplified physics model focuses on cutting, another important safety consideration **<C1>** is the possibility of the blade becoming entangled with dangling items such as hair. Contact with a strand of hair is not itself problematic; the concern arises only when hair becomes caught and begins to offer resistance to rotation, which could pull the hair as the motor continues to spin. This issue, at its core, is that a motor continues to spin even when it *encounters resistance*. In POV systems, such resistance can come from finger reach-throughs, hair, or other external disturbances. Fortunately, POV systems are also highly sensitive to changes in rotation speed due to the need to track timing precisely. This makes the detection of slowdowns due to external resistance straightforward. How sensitively the system detects external resistance can be adjusted by tuning the amount of slowdown that is tolerable. We have implemented the automatic stall detection for hair, as shown in Figure 28. The sensitivity was tuned so that normal taps do not interrupt rotation, while the slowdown due to hair entanglement can be detected within the time of one revolution (about 0.1s), after which the motor automatically stops. Alongside our recommendation to employ low-torque motors, automatic stall detection leverages how POV systems operate and can further minimize safety risks.

9.1.2 Improving Visual Smoothness at Safer Speeds. In general, higher speeds yield better visual smoothness. However, overly fast speeds may make the device unsafe. This issue can be mitigated by allowing the LEDs to span the full diameter rather than half, essentially doubling the display frequency without having to double the speed. Future designs could integrate LEDs and electrodes into a full-diameter line, improving visual smoothness at safer speeds.

9.2 Discussion of Recommended Conditions

We conducted a series of tests that measured different aspects of the sensing performance: spread, offset, response time, user experience,

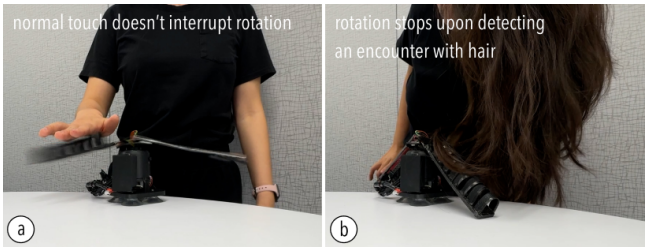


Figure 28: Automatic stall detection of external resistance with adjustable sensitivity. (a) Normal touch doesn't interrupt rotation, while (b) light external resistance, such as an encounter with hair, can be detected. Upon detection, the motor can automatically stop and optionally resume.

etc. We identified the significant factor (speed or electrode height) and recommended the best condition for each aspect.

Some of the best conditions may appear inconsistent when comparing the technical evaluation results and the user study results. For instance, 450 RPM yielded the minimal spread under controlled touches in the technical evaluation, whereas in the user study, 350 RPM yielded the minimal spread under varied real-world user touches. These results are not in conflict; they arise naturally from the different setups and touch behaviors. While we report the best condition from the technical evaluation, we primarily use user study results for recommendations to reflect real-world touches.

In some cases, different optimization goals favor different conditions. For example, a faster speed shows faster system response time, whereas a slower speed shows a smaller spread. While some divergence might be reconciled as the technology develops, some naturally introduce trade-offs, and the optimal configuration ultimately depends on the priorities of a specific application. Our study of individual aspects of POV-based touch displays gives future researchers a more comprehensive understanding and more specific goals for optimization. To help practitioners choose speeds and heights, we recommend high electrodes overall. For speeds, 450 RPM provides a better visual experience, while 350 RPM offers more accurate touch sensing.

9.3 Sensing Accuracy

We wish to stress that BloomBeacon is a first research prototype directly engaging with the key challenges of POV-based touch displays, and that there remains room for improvement. As an early hardware exploration, we assembled it with easily accessible parts. Looking ahead, we envision several opportunities to improve its sensing performance.

One limiting factor lies in our manual fabrication process, specifically, welding wires onto thin conductive TPU arches, which may introduce variability in conductance. We envision a streamlined industry process to address this.

Another limitation lies in our system's processing speed, governed by both the hardware and software. As POV systems are based heavily on stringent timing, high-speed sampling and processing would not only make the system more responsive, but also improve accuracy by minimizing touch spread due to small variations in detection latencies. Similar to how both hardware-centric [20, 28, 33, 37] and software-centric [15, 16, 36] solutions have significantly advanced the traditional touchscreen latency, both hardware and software solutions are needed for POV-based touch displays in future work. Sensors capable of sampling and processing touch signals at substantially higher rates would be directly beneficial. Complementarily, software solutions could develop fast, lightweight signal-processing algorithms tailored for noisy, brief contacts on spinning surfaces.

Knowing the *absolute* angular position when touch occurs can, in principle, significantly improve the sensing accuracy. In our system, as in most POV systems, the touch position is *not* tracked with absolute angular position, but is inferred by timing. As we mentioned in Section 3.3, the system only needs to detect the start of each revolution and divide the time for rotation into slices to reflect angles. This architecture offers several benefits: it uses components that return digital signals suitable for MCU interrupts, making it extremely fast. Tracking at the per-revolution level is also far less computationally demanding than at the per-degree level. The components it needs are also small, not adding bulk to the device. However, this architecture does not know the blade's actual angular position when a touch disturbs rotation mid-revolution, and only tracks the overall revolution slowdown and adjusts angular slicing until the new revolution starts. Therefore, an alternative architecture that could significantly improve angular accuracy is to use a motor encoder to obtain the absolute angular position. However, this would require the motor encoder to be extremely fast, far beyond the capabilities of typical encoders. For example, the motor we employ has an internal encoder that returns the real-time angular position. While the absolute angle reading is precise when the motor is turned very slowly, the sensor turned out to be too slow to catch up with the rotation speeds we need. While high-speed motor encoders might not be easily accessible at this time, we remain optimistic that future encoders that update at high speeds could offer an alternative hardware architecture that allows better angular accuracy.

9.4 Battery Life

One of the envisioned use cases is for users to flexibly augment the environment, and battery life is therefore an important design consideration, particularly since our display relies on motorized spinning. Conceptually, our system operates on demand: the display remains dormant and static when not in use, which helps preserve battery. During runtime, there are two major sources of power consumption: the LED display and the motor. The power consumption from the display side is less of a concern. Thanks to the POV effect, far fewer LEDs are needed compared to conventional screens, and a wide range of LED options, addressable or regular, offer different levels of power efficiencies. We are more interested in the consumption from the motor. In our system, at 450 RPM, the heaviest blade draws 0.07A. With the 7.4V, 400 mAh battery we use, this current draw corresponds to a motor runtime of about 5.7 hours (about 5 hours in practice to avoid battery depletion). For reference, an iPad 11's drain test [3] reports about 4 hours of continuous use. Looking ahead, with advancements in battery, motor, and LEDs, we believe improved system power efficiency is forthcoming.

[3] https://www.youtube.com/watch?v=atsQxdVlk7w

9.5 Context-Aware Interaction

One exciting future work lies in context-aware activation and interaction. When BloomBeacon is placed at different locations, it can potentially operate more intelligently by responding to its surroundings. For example, proxemics-aware sensing could allow the display to remain idle when no one is nearby, and activate only when users approach. Similarly, the device could be repositioned to different locations to display contextually relevant information. This also leads to another important future work of supporting user authoring and personalization. Because the display can be flexibly placed and relocated, there is a strong need for tools that allow users to customize what information is shown, where it appears, and how it behaves in different contexts. Such authoring interfaces would make BloomBeacon more versatile and user-driven, empowering people to augment their environments more flexibly.

9.6 Haptics Exploration

Our system also opens pathways for haptic exploration with such kinetic components. A unique benefit of our design is that the non-LED blade does not interfere with visuals formed by the LED blade, and the blades are swappable. This makes it possible to experiment with textured or geometric blade designs that provide richer tactile sensations. Inspired by work on parametric haptics [23], varying surface textures and geometries could expand the haptic expressiveness of the display and create opportunities for more nuanced physical feedback.

10 Conclusion

The goal of this work is to demonstrate the concept of blooming a touch display via Persistence-of-Vision motion, where the touch display surface emerges from a rotating line. The device mobility and on-demand expansiveness allow flexible placement and relocation for environmental augmentation. We identified and articulated three layers of challenges for the implementation of POV-based touch displays and proposed solutions and directions for each challenge. We also studied the key factors that affect various metrics of touching such spinning elements, and produced generalizable insights beyond a single device implementation. By establishing the generalizability on this type of blooming touch display, we open up more possibilities of where digital information and interaction can take place. As an initial exploration, it also makes clear that we are only at the beginning toward making physical interfaces dynamically 'bloom' in our everyday life, and the most exciting and challenging work lies ahead.

Acknowledgments

We thank Tucker Rae-Grant for his early contributions to the project. We also thank Anup Sathya, Romain Nith, and Pedro Lopes for their technical advice, as well as Ting-Han Lin and Anup Sathya for their detailed feedback on the manuscript. We are grateful to Yudai Tanaka for his expert guidance on statistical analysis and his in-depth feedback on the manuscript.

References

[1] [n. d.]. ASUKANET. https://www.asukanet.co.jp

[2] [n. d.]. Buy Galaxy Z Fold7 512GB | Blue Shadow Smartphone (Unlocked) | Price & Deals. https://www.samsung.com/us/smartphones/galaxy-z-fold7/buy/galaxy-z-fold7-512gb-unlocked-sku-sm-f966udbexaa/

[3] [n. d.]. Overview | CircuitPython Painter | Adafruit Learning System. https://learn.adafruit.com/circuitpython-painter/overview

[4] [n. d.]. POV Display Using Raspberry Pi Pico. https://www.hackster.io/H0meMadeGarbage/pov-display-using-raspberry-pi-pico-d6bc4f

[5] [n. d.]. References & Cases. https://www.fogscreen.com/audiovisual/fogscreenez-2/

[6] Waleed H Al-Natsheh, Bashar K Hammad, and Mustafa A Abu Zaid. 2019. Design and implementation of a cylindrical persistence of vision display. In *2019 6th International Conference on Electrical and Electronics Engineering (ICEEE)*. IEEE, 215–219.

[7] Jason Alexander, Anne Roudaut, Jürgen Steimle, Kasper Hornbæk, Miguel Bruns Alonso, Sean Follmer, and Timothy Merritt. 2018. Grand challenges in shape-changing interface research. In *Proceedings of the 2018 CHI conference on human factors in computing systems*. 1–14.

[8] amandaghassaei. [n. d.]. Persistence of Vision Wand. https://www.instructables.com/Persistence-of-Vision-Wand/

[9] Sif Fink Arnbjerg-Nielsen, Matthew D. Biviano, and Kaare H. Jensen. 2024. Competition between slicing and buckling underlies the erratic nature of paper cuts. *Physical Review E* 110, 2 (Aug. 2024), 025003. https://doi.org/10.1103/PhysRevE.110.025003 Publisher: American Physical Society.

[10] Peter C. Barnum, Srinivasa G. Narasimhan, and Takeo Kanade. 2010. A multi-layered display with water drops. In *ACM SIGGRAPH 2010 Papers* (Los Angeles, California) *(SIGGRAPH '10)*. Association for Computing Machinery, New York, NY, USA, Article 76, 7 pages. https://doi.org/10.1145/1833349.1778813

[11] Ferdinand P. Beer, E. Russell Johnston, John T. DeWolf, and David F. Mazurek. 2015. *Mechanics of Materials* (7 ed.). McGraw-Hill Education.

[12] Philipp Berens. 2009. CircStat: A MATLAB Toolbox for Circular Statistics. *Journal of Statistical Software* 31 (Sept. 2009), 1–21. https://doi.org/10.18637/jss.v031.i10

[13] Elodie Bouzbib, Iosune Sarasate, Unai Javier Fernández, Ivan Fernández, Manuel Lopez-Amo, Iñigo Ezcurdia, and Asier Marzo. 2025. FlexiVol: a Volumetric Display with an Elastic Diffuser to Enable Reach-Through Interaction. In *Proceedings of the 2025 CHI Conference on Human Factors in Computing Systems (CHI '25)*. Association for Computing Machinery, New York, NY, USA, Article 977, 16 pages. https://doi.org/10.1145/3706598.3714315

[14] Suzanne Buchan. 2013. *Pervasive Animation*. Routledge. Google-Books-ID: ZeiAAAAAQBAJ.

[15] Elie Cattan, Amélie Rochet-Capellan, and François Bérard. 2015. A Predictive Approach for an End-to-End Touch-Latency Measurement. In *Proceedings of the 2015 International Conference on Interactive Tabletops & Surfaces (ITS '15)*. Association for Computing Machinery, New York, NY, USA, 215–218. https://doi.org/10.1145/2817721.2817747

[16] Elie Cattan, Amélie Rochet-Capellan, Pascal Perrier, and François Bérard. 2015. Reducing Latency with a Continuous Prediction: Effects on Users' Performance in Direct-Touch Target Acquisitions. In *Proceedings of the 2015 International Conference on Interactive Tabletops & Surfaces (ITS '15)*. Association for Computing Machinery, New York, NY, USA, 205–214. https://doi.org/10.1145/2817721.2817736

[17] Rod Cross. 2014. Physics of bounce. *American Journal of Physics* 82, 3 (2014), 189–196.

[18] Marina Czerner, Laura A. Fasce, Josefa F. Martucci, Roxana Ruseckaite, and Patricia M. Frontini. 2016. Deformation and fracture behavior of physical gelatin gel systems. *Food Hydrocolloids* 60 (Oct. 2016), 299–307. https://doi.org/10.1016/j.foodhyd.2016.04.007

[19] Maxime Daniel and William Delamare. 2025. ShyPins: Safeguarding User Mental Safety From The Forcible (Dis)Appearance Of Pin-based Controls By Using Speed Zones. In *Proceedings of the Nineteenth International Conference on Tangible, Embedded, and Embodied Interaction*. ACM, Bordeaux/Talence France, 1–16. https://doi.org/10.1145/3689050.3704940

[20] Jonathan Deber, Ricardo Jota, Clifton Forlines, and Daniel Wigdor. 2015. How Much Faster is Fast Enough?: User Perception of Latency & Latency Improvements in Direct and Indirect Touch. In *Proceedings of the 33rd Annual ACM Conference on Human Factors in Computing Systems*. ACM, Seoul Republic of Korea, 1827–1836. https://doi.org/10.1145/2702123.2702300

[21] Stephen DiVerdi, Ismo Rakkolainen, Tobias Höllerer, and Alex Olwal. 2006. A novel walk-through 3D display. In *Stereoscopic Displays and Virtual Reality Systems XIII*, Vol. 6055. SPIE, 428–437.

[22] Werner Goldsmith. 2001. *Impact: The theory and physical behaviour of colliding solids*. Dover Publications.

[23] Violet Yinuo Han, Abena Boadi-Agyemang, Yuyu Lin, David Lindlbauer, and Alexandra Ion. 2023. Parametric Haptics: Versatile Geometry-based Tactile Feedback Devices. In *Proceedings of the 36th Annual ACM Symposium on User Interface Software and Technology (UIST '23)*. Association for Computing Machinery, New York, NY, USA, 1–13. https://doi.org/10.1145/3586183.3606766

[24] Chris Harrison, Hrvoje Benko, and Andrew D. Wilson. 2011. OmniTouch: wearable multitouch interaction everywhere. In *Proceedings of the 24th annual ACM symposium on User interface software and technology (UIST '11)*. Association for Computing Machinery, New York, NY, USA, 441–450. https://doi.org/10.1145/2047196.2047255

[25] Otmar Hilliges, David Kim, Shahram Izadi, Malte Weiss, and Andrew Wilson. 2012. HoloDesk: direct 3d interactions with a situated see-through display. In *Proceedings of the SIGCHI Conference on Human Factors in Computing Systems*. ACM, Austin Texas USA, 2421–2430. https://doi.org/10.1145/2207676.2208405

[26] Ryuji Hirayama, Diego Martinez Plasencia, Nobuyuki Masuda, and Sriram Subramanian. 2019. A volumetric display for visual, tactile and audio presentation using acoustic trapping. *Nature* 575, 7782 (Nov. 2019), 320–323. https://doi.org/10.1038/s41586-019-1739-5 Publisher: Nature Publishing Group.

[27] Hobby Projects. 2020. Vibration based LED POV Message Display. https://www.youtube.com/watch?v=s677zeW51k4

[28] Ricardo Jota, Albert Ng, Paul Dietz, and Daniel Wigdor. 2013. How fast is fast enough?: a study of the effects of latency in direct-touch pointing tasks. In *Proceedings of the SIGCHI Conference on Human Factors in Computing Systems*. ACM, Paris France, 2291–2300. https://doi.org/10.1145/2470654.2481317

[29] Hidetaka Katsuyama, Shio Miyafuji, and Hideki Koike. 2025. Spatially-unconstrained 3D Display: Dynamic Projection Mapping on Manipulable Rotating Objects. In *2025 IEEE Conference on Virtual Reality and 3D User Interfaces Abstracts and Workshops (VRW)*. 807–809. https://doi.org/10.1109/VRW66409.2025.00164

[30] Miu-Ling Lam, Bin Chen, Kit-Yung Lam, and Yaozhun Huang. 2014. 3D fog display using parallel linear motion platforms. In *2014 International Conference on Virtual Systems & Multimedia (VSMM)*. IEEE, 234–237.

[31] Hyunjae Lee, Sangyoung Cho, Jiwoo Hong, Geehyuk Lee, and Woohun Lee. 2014. JANUS. In *ACM SIGGRAPH 2014 Emerging Technologies* (Vancouver, Canada) *(SIGGRAPH '14)*. Association for Computing Machinery, New York, NY, USA, Article 15, 1 pages. https://doi.org/10.1145/2614066.2614098

[32] Jinha Lee, Alex Olwal, Hiroshi Ishii, and Cati Boulanger. 2013. SpaceTop: integrating 2D and spatial 3D interactions in a see-through desktop environment. In *Proceedings of the SIGCHI Conference on Human Factors in Computing Systems*. ACM, Paris France, 189–192. https://doi.org/10.1145/2470654.2470680

[33] Darren Leigh, Clifton Forlines, Ricardo Jota, Steven Sanders, and Daniel Wigdor. 2014. High rate, low-latency multi-touch sensing with simultaneous orthogonal multiplexing. In *Proceedings of the 27th annual ACM symposium on User interface software and technology*. ACM, Honolulu Hawaii USA, 355–364. https://doi.org/10.1145/2642918.2647353

[34] Diego Martinez Plasencia, Edward Joyce, and Sriram Subramanian. 2014. MisTable: reach-through personal screens for tabletops. In *Proceedings of the SIGCHI Conference on Human Factors in Computing Systems*. ACM, Toronto Ontario Canada, 3493–3502. https://doi.org/10.1145/2556288.2557325

[35] Yasuaki Monnai, Keisuke Hasegawa, Masahiro Fujiwara, Kazuma Yoshino, Seki Inoue, and Hiroyuki Shinoda. 2014. HaptoMime: mid-air haptic interaction with a floating virtual screen. In *Proceedings of the 27th annual ACM symposium on User interface software and technology*. 663–667.

[36] Mathieu Nancel, Stanislav Aranovskiy, Rosane Ushirobira, Denis Efimov, Sebastien Poulmane, Nicolas Roussel, and Géry Casiez. 2018. Next-Point Prediction for Direct Touch Using Finite-Time Derivative Estimation. In *Proceedings of the 31st Annual ACM Symposium on User Interface Software and Technology (UIST '18)*. Association for Computing Machinery, New York, NY, USA, 793–807. https://doi.org/10.1145/3242587.3242646

[37] Albert Ng, Julian Lepinski, Daniel Wigdor, Steven Sanders, and Paul Dietz. 2012. Designing for low-latency direct-touch input. In *Proceedings of the 25th annual ACM symposium on User interface software and technology (UIST '12)*. Association for Computing Machinery, New York, NY, USA, 453–464. https://doi.org/10.1145/2380116.2380174

[38] Aditya Patel, Ashish Kumar Khandual, Kavya Kumar, and Shreya Kumar. 2015. Persistence Of Vision Display-A Review. *IOSR Journal of Electrical and Electronics Engineering (IOSR-JEEE) e-ISSN* 10, 4 (2015), 36–40.

[39] Claudio Pinhanez. 2001. The Everywhere Displays Projector: A Device to Create Ubiquitous Graphical Interfaces. In *Ubicomp 2001: Ubiquitous Computing*, Gregory D. Abowd, Barry Brumitt, and Steven Shafer (Eds.). Springer, Berlin, Heidelberg, 315–331. https://doi.org/10.1007/3-540-45427-6_27

[40] Diego Martinez Plasencia, Ryuji Hirayama, Roberto Montano-Murillo, and Sriram Subramanian. 2020. GS-PAT: high-speed multi-point sound-fields for phased arrays of transducers. *ACM Trans. Graph.* 39, 4, Article 138 (Aug. 2020), 12 pages. https://doi.org/10.1145/3386569.3392492

[41] Isabel PS Qamar, Rainer Groh, David Holman, and Anne Roudaut. 2018. HCI meets material science: A literature review of morphing materials for the design of shape-changing interfaces. In *Proceedings of the 2018 CHI Conference on Human Factors in Computing Systems*. 1–23.

[42] Ismo Rakkolainen, Tobias Höllerer, Stephen DiVerdi, and Alex Olwal. 2009. Mid-air display experiments to create novel user interfaces. *Multimedia Tools and Applications* 44, 3 (Sept. 2009), 389–405. https://doi.org/10.1007/s11042-009-0280-1

[43] Majken K Rasmussen, Esben W Pedersen, Marianne G Petersen, and Kasper Hornbæk. 2012. Shape-changing interfaces: a review of the design space and open research questions. In *Proceedings of the SIGCHI Conference on Human Factors in Computing Systems*. 735–744.

[44] Simon Robinson, Céline Coutrix, Jennifer Pearson, Juan Rosso, Matheus Fernandes Torquato, Laurence Nigay, and Matt Jones. 2016. Emergeables: Deformable displays for continuous eyes-free mobile interaction. In *Proceedings of the 2016 CHI Conference on Human Factors in Computing Systems*. 3793–3805.

[45] Gazelle Saniee-Monfared, Kevin Fan, Qianq Xu, Sachi Mizobuchi, Lewis Zhou, Pourang Polad Irani, and Wei Li. 2020. Tent Mode Interactions: Exploring Collocated Multi-User Interaction on a Foldable Device. In *22nd International Conference on Human-Computer Interaction with Mobile Devices and Services*. ACM, Oldenburg Germany, 1–12. https://doi.org/10.1145/3379503.3403566

[46] Stefan Schneegass, Florian Alt, Jürgen Scheible, and Albrecht Schmidt. 2014. Midair displays: Concept and first experiences with free-floating pervasive displays. In *Proceedings of The International Symposium on Pervasive Displays*. 27–31.

[47] Oliver A. Shergold and Norman A. Fleck. 2005. Experimental Investigation Into the Deep Penetration of Soft Solids by Sharp and Blunt Punches, With Application to the Piercing of Skin. *Journal of Biomechanical Engineering* 127, 5 (Feb. 2005), 838–848. https://doi.org/10.1115/1.1992528

[48] Miriam Sturdee and Jason Alexander. 2019. Analysis and Classification of Shape-Changing Interfaces for Design and Application-based Research. *Comput. Surveys* 51, 1 (Jan. 2019), 1–32. https://doi.org/10.1145/3143559

[49] Yura Tamai, Maho Oki, and Koji Tsukada. 2021. POV Display and Interaction Methods extending Smartphone. In *Proceedings of the Augmented Humans International Conference 2021* (Rovaniemi, Finland) *(AHs '21)*. Association for Computing Machinery, New York, NY, USA, 183–191. https://doi.org/10.1145/3458709.3458992

[50] Nicolas Villar, Daniel Cletheroe, Greg Saul, Christian Holz, Tim Regan, Oscar Salandin, Misha Sra, Hui-Shyong Yeo, William Field, and Haiyan Zhang. 2018. Project Zanzibar: A Portable and Flexible Tangible Interaction Platform. In *Proceedings of the 2018 CHI Conference on Human Factors in Computing Systems*. ACM, Montreal QC Canada, 1–13. https://doi.org/10.1145/3173574.3174089

[51] Robert Xiao, Chris Harrison, and Scott E. Hudson. 2013. WorldKit: rapid and easy creation of ad-hoc interactive applications on everyday surfaces. In *Proceedings of the SIGCHI Conference on Human Factors in Computing Systems (CHI '13)*. Association for Computing Machinery, New York, NY, USA, 879–888. https://doi.org/10.1145/2470654.2466113

[52] Vasco Xu and Ken Nakagaki. 2023. Xs: Interactive Scissor Mechanisms as Portable and Customizable Shape-Changing Interfaces. In *Proceedings of the Seventeenth International Conference on Tangible, Embedded, and Embodied Interaction (TEI '23)*. Association for Computing Machinery, New York, NY, USA, 1–10. https://doi.org/10.1145/3569009.3572737

[53] Wataru Yamada, Kazuhiro Yamada, Hiroyuki Manabe, and Daizo Ikeda. 2017. iSphere: Self-Luminous Spherical Drone Display. In *Proceedings of the 30th Annual ACM Symposium on User Interface Software and Technology*. ACM, Québec City QC Canada, 635–643. https://doi.org/10.1145/3126594.3126631

[54] Willa Yunqi Yang, Yumeng Zhuang, Luke Andre Darcy, Grace Liu, and Alexandra Ion. 2022. Reconfigurable elastic metamaterials. In *Proceedings of the 35th Annual ACM Symposium on User Interface Software and Technology*. 1–13.

[55] Willa Yunqi Yang, Yifan Zou, Jingle Huang, Raouf Abujaber, and Ken Nakagaki. 2024. TorqueCapsules: Fully-Encapsulated Flywheel Actuation Modules for Designing and Prototyping Movement-Based and Kinesthetic Interaction. In *Proceedings of the 37th Annual ACM Symposium on User Interface Software and Technology*. 1–15.

[56] Takumi Yoshida, Sho Kamuro, Kouta Minamizawa, Hideaki Nii, and Susumu Tachi. 2010. RePro3D: full-parallax 3D display using retro-reflective projection technology. In *ACM SIGGRAPH 2010 Emerging Technologies*. ACM, Los Angeles California, 1–1. https://doi.org/10.1145/1836821.1836841

[57] Takatoshi Yoshida, Yoshihiro Watanabe, and Masatoshi Ishikawa. 2016. Phyxel: Realistic Display of Shape and Appearance using Physical Objects with High-speed Pixelated Lighting. In *Proceedings of the 29th Annual Symposium on User Interface Software and Technology*. ACM, Tokyo Japan, 453–460. https://doi.org/10.1145/2984511.2984548

[58] Jiakun Yu, Supun Kuruppu, Biyon Fernando, Praneeth Bimsara Perera, Yuta Sugiura, Sriram Subramanian, and Anusha Withana. 2024. IrOnTex: Using Ironable 3D Printed Objects to Fabricate and Prototype Customizable Interactive Textiles. *Proceedings of the ACM on Interactive, Mobile, Wearable and Ubiquitous Technologies* 8, 3 (2024), 1–26.